The host galaxies of long gamma-ray bursts

Kim Lewis John Tibbetts-Harlow

Supervisors:

Nial Tanvir

Andrew Blain

Thesis to be submitted for the degree of

Master of Philosphy

at the University of Leicester

X-ray & Observational Astronomy Group

Department of Physics and Astronomy

University of Leicester

January 27, 2015

The host galaxies of long gamma-ray bursts

Kim Lewis John Tibbetts-Harlow

ABSTRACT

This thesis presents Hubble Space Telescope (*HST*) infra-red imaging of the locations of 40 *Swift* detected long gamma-ray bursts (LGRBs) with known redshifts $z < 3$ and subsequent analysis.

Of the 40 imaged, host galaxy detections are obtained in 35 cases and upper limits in the remaining 5. For the 35 detected hosts, there is sufficient quality data to locate the LGRB to better than an *HST* pixel ($\sim 0.13''$) precision in 30 cases.

Data on the burst locations is shown, as well as on the photometry and morphology of their host galaxies. Also shown is that the distribution of bursts with respect to the light distribution of their hosts is similar in the infra-red to that already measured by previous work in the optical.

Acknowledgments

Thank you to those colleagues at Leicester who were always willing to give patient help and advice, and to let me benefit from their years of experience, especially Phil and Klaas who had the patience of saints.

A special thank you to Nial Tanvir, without whom this thesis would probably not exist. His patience, support and guidance was all I could have asked for and more, and I will always consider myself lucky to have had him as my supervisor.

And, of course, thank you to my family, without whom none of this would have been possible.

Declaration

I hereby declare that no part of this thesis has been previously submitted to this or any other University as part of the requirement for a higher degree. The work described herein was conducted by the undersigned except for contributions from colleagues as acknowledged in the text.

Kim Tibbetts-Harlow
January 27, 2015

Contents

List of Tables

List of Figures

1 Introduction

1.1 The discovery of gamma-ray bursts

Gamma-ray bursts (GRBs) are intense flashes of gamma-rays. They were first detected in 1967 by the U.S. military's *Vela* satellites, designed to monitor for illicit nuclear explosions in contravention of the Nuclear Test Ban Treaty (Klebesadel et al., 1973). However, while the satellites had sufficient spatial resolution to rule out solar or terrestrial origins for the bursts, they were unable to locate obvious sources for the bursts, despite performing a search for associated novae or supernovae. In the following years many different theories were proposed for GRBs' origins (e.g. Tremaine & Zytkow, 1986; Blaes et al., 1989; Haensel et al., 1991; Usov, 1992), however it wasn't until the Burst and Transient Source Explorer instrument (BATSE) became available following the launch of the *Compton Gamma Ray Observatory* in 1991 that the next significant observational progression was made.

BATSE observed an isotropic distribution of gamma-ray bursts on the sky as seen in figure 1.1, strongly disfavouring a Galactic origin (Meegan et al., 1992). This led to a variety of new theories as to the GRBs' progenitors. However, once again observational progress stalled: for

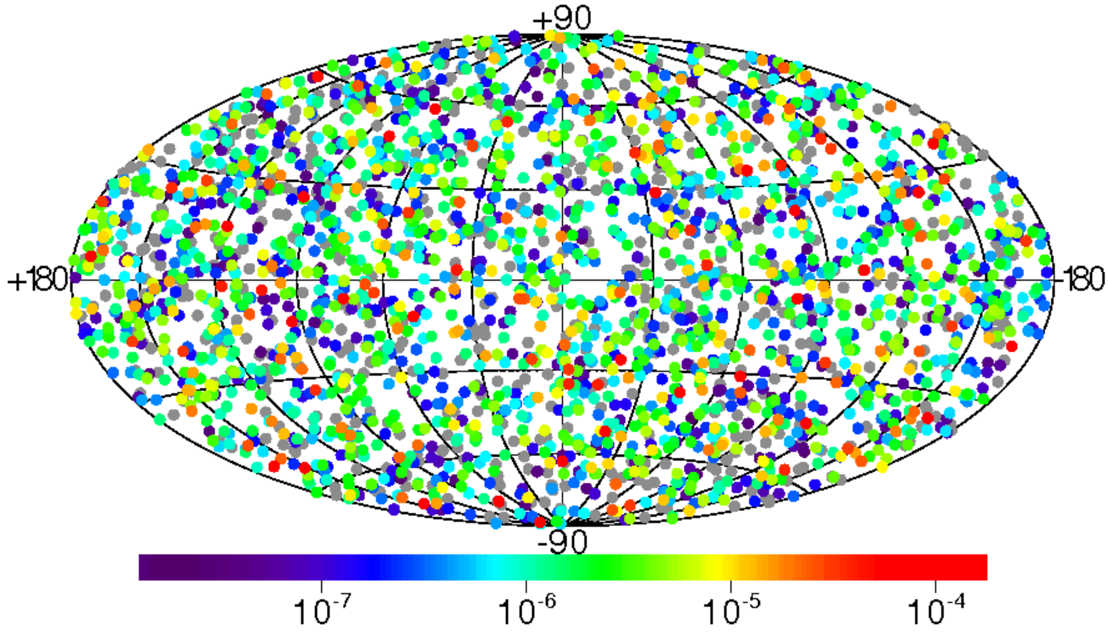

Figure 1.1: Distribution of all 2704 GRBs detected by the BATSE instrument on the *Compton Gamma-Ray Observatory* in galactic coordinates. (Colour of dots represents gamma-ray fluence in the 50-100 keV band in $ergs\ cm^{-2}$, with red being the most energetic bursts). The distribution is apparently isotropic there is no obvious clustering of bursts along the galactic plane or towards the galactic centre. Original image from http://www.batse.msfc.nasa.gov/batse/grb/skymap/

years all attempts to identify the sources of the bursts failed (with the exception of one event now not considered a GRB[1]). However, this event was recognised at the time as an atypical burst and is now believed to have been a magnetar giant flare rather than a GRB.

The next big breakthrough was made in 1997 following the Italian-Dutch satellite *BeppoSAX*'s (Boella et al., 1997) launch in 1996, with its combination of wide and narrow field instruments allowing for detection and follow-up respectively. After *BeppoSAX* detected GRB 970228[2], spatially coincident fading X-ray (Costa et al., 1997) and optical (van Paradijs et al., 1997) sources were detected in the error circle of the gamma-ray detection. Follow up images detected a faint galaxy at this position (van Paradijs et al., 1997; Sahu et al., 1997), giving further strong support to theories of a cosmological origin for GRBs (e.g. Paczynski, 1986). A few months later GRB 970508 strengthened them yet further as spectroscopy of its afterglow

[1] A pair of GRB-like events were observed a day apart in March 1979 from the same source, which were spatially coincident with a supernova remnant in the Large Magellanic Cloud (Mazets et al., 1979; Cline et al., 1980)

[2] GRBs are named after the year/month/day they were discovered in the UT timezone using a YYMMDD format, so GRB 970228 was discovered on the 28th of February 1997. If more than one GRB is detected in the same day, letters A, B, C etc are appended to the end in the order they were publicly announced: for example GRB 100316D was the fourth announced GRB detected on the 16th of March 2010.

revealed absorption features at a redshift $z = 0.835$ (Metzger et al., 1997). While it was impossible to say whether the absorbing matter was associated with the GRB or any host galaxy, it placed a firm lower limit on the burst's redshift. A lack of Lyman-alpha forest[3] features further allowed Metzger et al., 1997 to place an upper limit of $z \sim 2.3$. Later *Hubble Space Telescope* (*HST*) imaging once the afterglow had faded revealed a spatially coincident galaxy at a redshift of $z = 0.83$, presumably the host of the GRB (Fruchter et al., 2000).

Further observations by multiple satellites have since increasingly widened our understanding of GRBs. The *Compton Gamma Ray Observatory* (with BATSE attached) functioned until it was deorbitted in 2000. Likewise, *BeppoSAX* functioned until 2002 and was destroyed re-entering the Earth's atmosphere in 2003. *HETE-2*[4] functioned from 2000 to 2006, using gamma-ray, X-ray and UV instruments to locate the GRB first via the initial gamma-ray pulse and then accurately pin down its location using the X-ray and optical afterglow to within as little as 3 arcseconds for particularly bright bursts. In 2004, the *Swift* satellite (Gehrels et al., 2004) launched and is still operational today, and has detected more than 500 GRBs. Like *HETE-2*, *Swift* is equipped with detectors sensitive in the gamma-ray, X-ray and UV portions of the spectrum, and combined with its ability to slew to new targets very rapidly to point its X-ray and UV cameras at the location of a GRB detected using the wide-field gamma-ray detector. This allows accurate X-ray positions typically less than a minute after the initial gamma-ray detection, and has allowed *Swift* to get X-ray positions for more than 90% of its bursts. The accuracy of these X-ray positions is enough to search for the afterglow with other ground and space-based instruments even if the UV camera fails to detect it, and has as a result allowed redshift determinations for over 150 GRBs. Further information about the properties of GRBs, particularly at high energies, has also recently been provided by the new *Fermi Gamma-Ray Space Telescope* launched in 2008.

[3]Spectra of high redshift objects show a series of absorption lines called the Lyman-alpha forest, caused by multiple intervening neutral hydrogen clouds at different redshifts creating a forest of absorption lines. The location, or lack-thereof, of this feature can be used to constrain the redshift of a source.

[4]The original *HETE* was lost at launch due to a rocket malfunction in 1996. *HETE-2* was then built following the same design, and was finally successfully launched four years later.

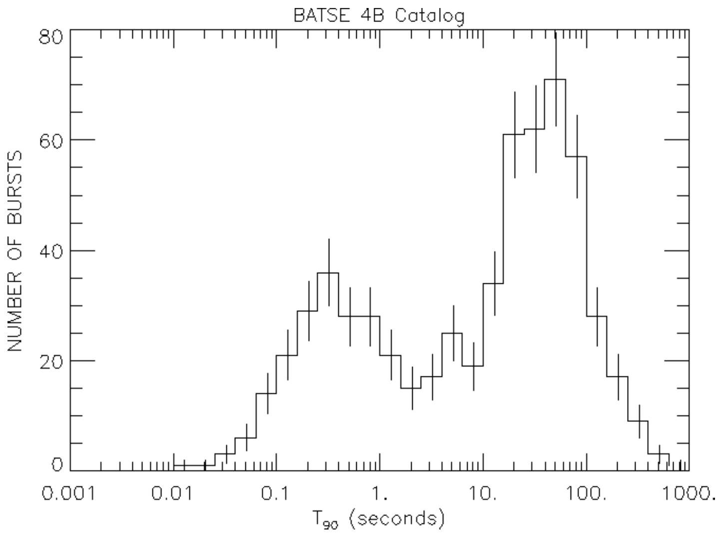

Figure 1.2: Histogram of the burst length (t_{90}) of all BATSE detected GRBs. A bimodal distribution is clearly apparent. Image from http://www.batse.msfc.nasa.gov/batse/grb/duration/

1.2 Two distinct populations

One key discovery made early on in the study of GRBs is that there appear to be two distinct populations (Kouveliotou et al., 1993), roughly divided by length of the initial gamma-ray pulse (specifically the t_{90} of the pulse, that is the time in which the middle 90% of the high energy counts from the GRB arrive in the detector, i.e. the length of the high energy burst once the first and last 5% of the burst's counters are discarded). This is most clearly seen in a histogram of the burst length of BATSE detected GRBs, as shown in figure 1.2. The two classes of GRBs are generally defined as short GRBs (SGRBs), with $t_{90} < 2$ s, and long GRBs (LGRBs) with $t_{90} > 2$ s. This two population model is also apparent in hardness, as shorter bursts seem to be harder than longer bursts (Fishman, 1999). However, as can be seen in figure 1.2 there is a large overlap between the two categories, so it can be hard to conclusively categorise many bursts based on duration alone. A further difference between the two classes of GRBs and a significant clue to differing origins is shown by the host galaxies of the bursts.

1.2.1 Short gamma-ray bursts

SGRBs are found to be associated with a wide variety of galaxy morphologies, including those with little or no star formation such as elliptical galaxies, and are often found offset from their host galaxies (e.g. Gehrels et al., 2005; Bloom et al., 2006b; Berger et al., 2005b; Berger, 2009; Fong et al., 2010). On the other hand, the typical LGRB host galaxy is a young, faint star forming galaxy (Christensen et al., 2004). Furthermore LGRBs are sometimes associated with supernovae (SNe), whereas SN searches have failed to detect any SNe connected to SGRBs to deep limits (for a detailed review of the SN-GRB connection see Woosley & Bloom, 2006). It is therefore believed that LGRBs and SGRBs have different progenitors, but that the gamma-ray and afterglow emission itself is caused by the same mechanism.

Because SGRBs are found in a variety of environments of varying ages and star formation rates, from young star forming galaxies to giant ellipticals, they are not believed to be associated with star formation. The leading theory for SGRB progenitors is that they are caused by double neutron star mergers (NS-NS) or neutron star and black-hole mergers (NS-BH) (e.g. Paczynski, 1991; Narayan et al., 1992). As there are potentially Gyr timescales between the stellar birth and resulting supernovae and the eventual NS-NS merger, there is no need for SGRBs to be associated with recent star formation. Furthermore, the theory predicts that some binary systems will receive large velocity “kicks” relative to their host galaxies when the neutron stars form via core collapse SNe (Bloom et al., 1999; Fryer et al., 1999; Belczynski et al., 2006); such velocities, combined with the merger time of NS-NS and NS-BH systems, mean that binaries may escape their host galaxies before the SGRB occurs, explaining why some SGRBs are found offset from their host galaxies. The situation can also be complicated by other sources of bursts of gamma rays, such as flaring magnetars or tidal distruption flares (e.g. (Castro-Tirado et al., 2008) and (Cenko et al., 2012)).

1.2.2 Long gamma-ray bursts

LGRBs are observed to originate from young and often small star forming galaxies (see e.g. Svensson et al., 2010), and in some cases are detected in association with spatially and temporally coincident core-collapse supernovae (SNe) (see Hjorth & Bloom, 2012 and references therein for a review of the evidence for the GRB-SN connection). As a result, they are believed to be associated with the collapse of some massive stars (Woosley, 1993a, 1996; MacFadyen & Woosley, 1999) - however the mechanism which causes only some stars to form LGRBs is not fully known. Detailed study of the galaxies that host LGRBs, and the locations within the galaxies that bursts occur, provides a route to understanding what causes some stars to create LGRBs at the end of their lives, and what special conditions are required, if any, for a star's evolution to end with a LGRB rather than a more typical core-collapse SN.

Previous work has attempted to quantify the similarity between LGRBs and SNe. LGRBs are typically found in star forming galaxies, and are often found in the brightest star forming regions of their hosts, implying that they are strongly associated with star formation, more so than typical core collapse SNe, and are also typically found in smaller and more irregular host galaxies (Fruchter et al., 2006; Svensson et al., 2010).

However, in terms of the degree to which they track the light of their hosts, LGRBs are more comparable to type Ic SNe (core collapse SNe lacking hydrogen or helium lines) (Kelly et al., 2008), and some LGRBs have been associated with type Ic SNe (e.g. SN 2003dh/GRB 030329 (Mazzali et al., 2003), SN 2010bh/GRB 100316D (Chornock et al., 2010), SN 2013cq/GRB 130427A (Xu et al., 2013)), . It is currently believed that LGRBs are a subclass of type Ic SNe caused by the collapse of massive (initial masses of at least thirty solar masses), rapidly rotating Wolf-Rayet stars (Woosley, 1993b). This requirement for especially massive progenitor stars naturally explains the strong association with star formation, as massive stars are found almost exclusively in areas with high recent star formation rates. There is also evidence for a metallicity dependence for LGRBs, or at least a preference to lower metallicity environments (e.g. Stanek et al., 2006; Wolf & Podsiadlowski, 2007; Levesque et al., 2010), although the exact nature of this dependance is yet to be conclusively quantified (e.g. Savaglio et al., 2009).

1.3 The fireball model

While SGRBs and LGRBs are believed to be caused by very different progenitors, on very different timescales (from NS-NS mergers inspiralling over Gyrs to "hypernovae" of stars with lifetimes of the order Myrs), the emission mechanisms of the gamma-rays and afterglows are believed to be the same, as would be expected by the apparent similarity. The leading candidate

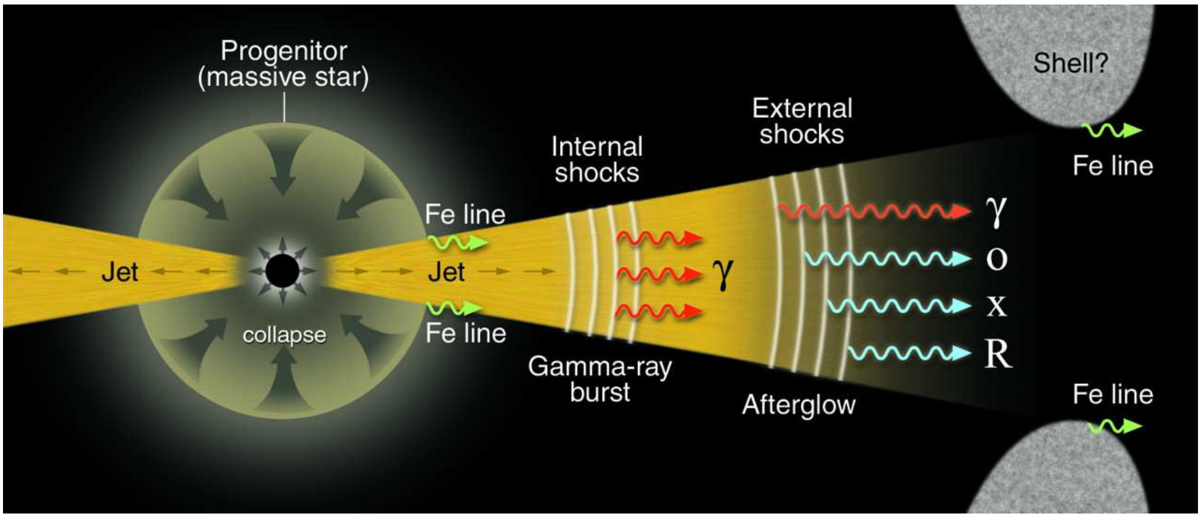

Figure 1.3: Schematic diagram of the fireball model, taken from Meszaros, 2001.

is the "fireball model" (Rees & Meszaros, 1992; Meszaros & Rees, 1993), in which a fireball of electrons, positrons and gamma-ray photons expands relativisticly from the collapsing system (either the NS-NS/NS-BH merger of SGRBs or the centre of a Wolf-Rayet star in the process of collapsing to a black-hole). As observed GRB fluxes imply energies up to 10^{54} erg (Meszaros, 2001) (roughly equivalent to the rest mass energy of the Sun!) it is believed this fireball is collimated into a relativistic jet, as a result of which we only see the small portion of GRBs in which the jet is pointed towards us. This jet then undergoes internal shocks, releasing a pulse of gamma-rays which we see as the GRB, although as the collapse is not instantaneous, especially in the case of LGRBs, this emission continues for a finite period of time and may even show multiple peaks. As the jet then proceeds to collide with the interstellar medium it decelerates, creating external shocks which lead to the afterglow, initially in gamma-ray energies but quickly falling off to X-ray, optical and eventually radio emission. A schematic of this process is shown in figure 1.3, specifically for a LGRB.

1.4 LGRBs as probes of the evolution of galaxies and the Universe

LGRBs offer a unique probe of the early Universe. While the most distant deep-field selected galaxy candidates ever detected are at photometric redshifts of $z \sim 8$ and possibly out to $z \sim 12$ in the Hubble Ultra-Deep Field (Bouwens et al., 2011; Ellis et al., 2013), LGRBs have been detected at spectroscopic redshifts of up to $z = 8.2$ (Tanvir et al., 2009; Salvaterra et al., 2009) and photometric redshifts of up $z \sim 9.4$ (Cucchiara et al., 2011). Furthermore, the brightest LGRBs should be detectable at redshifts of up to $z > 20$ (e.g. Gou et al., 2004; Bloom et al., 2009). At higher redshifts, when average metallicities were significantly lower (beyond $z \sim 2$ average metallicities may have been less than a tenth of what they are now, see e.g. Lu et al., 1996; Savaglio et al., 2005), any metallicity dependence for LGRBs may prove negligible, LGRBs may provide an almost unbiased tracer of massive star formation (Fynbo et al., 2008d), however future work and better understanding of the typical environments of LGRBs, from samples such as this one, will be required to quantify any effect. If true, this means that LGRBs would provide a valuable tool for selecting samples of high redshift galaxies without the traditional biases associated with galaxy selection (see e.g. Smail et al., 2011; Stringer et al., 2011); an LGRB selected sample also has the added benefit that one knows each galaxy's redshift and position, from afterglow spectroscopy or photometry[5], before one tries to observe it, and smaller, less-massive galaxies will be included in the sample, even if only as host non-detections and associated photometric upper limits (see e.g. Basa et al., 2012; Tanvir et al., 2012; Trenti et al., 2012). Being able to quantify the lower end of the luminosity function would be an invaluable contribution to our understanding of heirachical galaxy formation in the early Universe and the contribution of smaller galaxies to the reionisation of the Universe, as most studies are only able to probe bright, high mass end of the function (see e.g. Cole et al., 2001).

[5]Photometric redshifts require an assumption of the source's spectral energy distribution (SED). As GRB afterglows have simple and predictable SEDs, photometric redshifts of GRBs are generally more reliable than those of galaxies, which have significantly differing SEDs from one source to another.

1.5 This thesis

Before LGRBs can be used effectively as probes, it is vital to understand what is required for an LGRB to occur, which can be investigated by understanding the environments these bursts occur in. As LGRBs are strongly associated with star formation and typically associated with low metallicity environments, typical LGRB hosts are small, faint and blue in colour. Most previous studies (e.g. Fruchter et al., 2006) have been conducted in the rest-frame UV and optical, where the hosts are brightest. However, at these wavelengths, the galaxy's flux is dominated by the youngest, brightest stars. As LGRB hosts are typically very strongly star forming, this results in measurements such as galaxy morphology being strongly distorted by star forming regions within the galaxy. In the near infra-red (NIR) this problem is less pronounced, so in order to study the hosts of LGRBs and where within of them LGRBs occur, NIR studies are also vital. Unfortunately, the faint and blue nature of LGRB hosts makes this a difficult prospect from the ground, so previous NIR studies have suffered from non-detections of significant proportions of their targets (e.g. Le Floc'h et al., 2003; Hjorth et al., 2012)[6], resulting in an incomplete picture and limiting any quantitative conclusions about the whole population. Therefore, in order to probe LGRB hosts at NIR wavelengths effectively, the *Hubble Space Telescope* (*HST*) is needed.

This thesis presents a survey of the hosts of 40 historic LGRBs[7] detected by *Swift*, all with known redshifts, imaged in the NIR by *HST*. This represents the largest and one of the most homogeneous sample of LGRB hosts yet imaged in the NIR (although see discussion in Section 2.2.1 about the sample's homogeneity). This sample includes 35 host galaxy detections, for 30 of which the burst location on the image is known to better than an *HST* pixel in accuracy (which in the H band corresponds to $\sim 0.13''$). The limitations typically prevalent in surveys of this nature due to preferential detection of brighter hosts are significantly

[6] Hjorth et al., 2012 did not require a redshift for their candidates, so represent a more homogeneous sample of targets than our survey

[7] While 43 burst locations were imaged, only 40 were fully used for the analyses in this paper. Of the remaining three bursts, one has had its redshift later withdrawn, the previously published redshift of one is shown to be incorrect by this work and the image for one is seriously degraded due to a "smearing" effect from a loss of tracking on *HST*. For this reason these three images are excluded from the results in this paper, however they are included in the data tables in the hope that the data will be of use to others.

reduced by this 87.5% detection rate[8]. Furthermore, the size of this sample will form the basis for future statistical analyses to be performed both of the hosts themselves and of the burst locations.

This thesis uses the AB-magnitude system (Oke & Gunn, 1983) and adopts a standard Λ-CDM cosmology with $H_0 = 71\ \mathrm{kms^{-1}Mpc^{-1}}$, $\Omega_M = 0.27$ and $\Omega_\Lambda = 0.73$ (Jarosik et al., 2011).

[8] *cf.* the 60% and 42% detection rates of Le Floc'h et al. (2003) and Hjorth et al. (2012) respectively.

2

An HST SNAPSHOT sample of long gamma-ray burst host galaxies in the infra-red

2.1 Chapter overview

With the aim of better understanding the host galaxies of long gamma-ray bursts (LGRBs), *Hubble Space Telescope* (*HST*) infra-red imaging of the locations of 40 *Swift* detected LGRBs with known redshifts $z < 3$. Within this sample, 35 host galaxy detections and 5 upper limits were obtained. For the 35 detected hosts, there was sufficient quality data to locate the LGRB to better than an *HST* pixel ($\sim 0.13''$) precision in 30 cases.

This chapter provides data on the burst locations, and on the photometry and morphology of their host galaxies. It is also shown that distribution of bursts with respect to the light distribution of their hosts is similar in the infra-red to that already measured by previous work in the optical.

2.2 Observations and analysis

2.2.1 The Snapshot proposal

Under *HST* Snapshot programmes, a large number of potential imaging targets are supplied and a portion of them are imaged in down-time between longer observations. This paper reports results from *HST* Proposal 12307 (PI: Levan), the *HST* has gathered a snapshot imaging sample of GRB host galaxies. The original list of potential targets consisted of a list of GRBs detected by *Swift*, all with reported redshifts $z \leq 3$ measured either from the afterglow or from spectroscopy of a presumed host; *HST* images of the locations of 40 LGRBs have so far been taken, spanning a range from $z = 0.03345$ to $z = 2.9$. All the images were taken with the WFC3 instrument in the F160W filter which corresponds to the H-band in the near-infrared. Three different exposure times were used depending on the distance of the LGRB host: the locations of LGRBs at $z \leq 1$ were imaged for 15 minutes, those at $1 < z \leq 2$ were imaged for 20 minutes and those at $2 < z \leq 3$ were imaged for approximately 27 minutes. This allowed for more images to be acquired while still attaining sufficient depth to detect the higher redshift LGRB hosts.

The proposal's aim was to create a catalogue of the properties of GRB hosting galaxies, such as their colours, luminosities and morphologies, in order to allow us to better understand the nature of the progenitors and how LGRBs can be used to understand star formation rates across a wide range of redshifts. In addition it also aimed to ensure the data would be useful in future research.

As the potential targets of the sample consisted of detected by *Swift* with a reported redshifts $z \leq 3$, our sample lacks the usual biases against faint galaxies in galaxy surveys, as we can easily quantify the host non-detection rate. However, the redshift requirement introduces a potential bias against particularly dusty hosts (which are less likely to have measured redshifts due to fainter afterglows).

The result is the largest and one of the most homogeneous sample of near-infrared detected LGRB hosting galaxies yet created. For nearby galaxies ($z \lesssim 1.5$) the observed band corresponds to rest-frame NIR, affording us a much better picture of the older stellar populations and presenting an image of the galaxy which is less dominated by the youngest and brightest stars. This gives a more accurate view of underlying galaxy morphology, and is likely particularly significant in LGRB hosting galaxies as the burst is likely itself evidence of recent star formation, thus biasing LGRB hosting galaxies to having more recent star formation than typical field galaxies. For the more distant galaxies ($z \gtrsim 1.5$), we are looking at rest frame optical light, giving us a useful sample to compare with lower redshift optical samples to understand any redshift evolution in the nature of LGRB hosting galaxies.

Table 2.1 contains a list of all the LGRBs imaged in this program, along with a variety of properties of the burst already known from the prompt emission and afterglow. Notes on the table: (a) Quoted redshift is of an extended object which almost certainly isn't the host galaxy; (b) LGRB location is very near a bright foreground star, increasing photometric errors; (c) *HST* guide star acquisition failed during this pointing, resulting in a badly "blurred" imaged; (d) redshift later withdrawn, now only known to be at $z < 3$; (e) tentative spectroscopic supernova association.

Figure 2.1 shows the redshift distribution of all the LGRBs. As is clearly visible in Figure 2.1, there are more bursts in the sample at lower redshifts. The distribution reflects that of the input sample, but is biased by the snapshot nature of the program and variable exposure times described earlier, resulting in bursts in lower redshift brackets being more likely to be scheduled, as they require shorter exposure times and therefore can be more easily fit into the *HST* schedule.

2.2.2 Image analysis - astrometry and photometry

For each image, we want to locate exactly where on the *HST* image the LGRB went off, both to firmly identify the host galaxies but also to pinpoint the exact location of the burst within the host galaxy for further analysis later. As the goal is not just to isolate the burst to a particular galaxy but to area of that galaxy, a subpixel accuracy position is desirable (for clarity, unless otherwise specified, "pixel" and associated words such as "sub-pixel" will refer to an *HST* pixel in size, which in the H band corresponds to $\sim 0.13''$).

In order to obtain the most accurate possible GRB position on the *HST* images, the best

GRB	z	z type	t_{90} (s)	NH ($\times 10^{21}$) (cm^{-2})	A_H (mag)	Exp. time (s)	Assoc. SN?	References	Notes
050315	1.949	spec	95.6	8.7	0.022	1209			
050401	2.898	spec	33.3	11.4	0.029	1612		(2) (3) (4)	
050406	2.7	host	5.4	0	0.01	1612			
050803	?	n/a	87.9	1.87	0.033	906			(a)
050824	0.828	spec	22.6	0.37	0.016	906	phot	(6) (4)	
051016B	0.936	spec	4	6.27	0.017	906			
060124	2.3	spec	~ 750	6.5	0.061	1612		(8) (9) (10) (4)	(b)
060218	0.033	spec	~ 2100	3.42	0.064	906	spec		(b)
060502A	1.503	spec	28.4	4.8	0.015	1209		(12) (4)	
060505	0.089	spec	~ 4	0.81	0.009	906		(13) (5)	
060512	2.1	spec	8.5	0	0.008	906		(14) (4)	(c)
060602A	0.787	host	75	11.4	0.011	906		(15) (5)	
060614	0.126	spec	108.7	0.29	0.01	906		(16) (4)	
060729	0.543	spec	115.3	1.45	0.024	906	phot	(17) (4)	
060912A	0.937	host	5	0.99	0.024	906			
061007	1.262	spec	75.3	4.84	0.009	1209		(19) (4)	
061110A	0.758	spec	40.7	2	0.041	906		(20) (21) (4)	
070318	0.84	spec	74.6	8.06	0.008	906		(22) (4)	
070508	< 3	n/a	20.9	4.62	0.062	906		(23) (4)	(d)
070521	1.35	ph(host)	37.9	16.6	0.012	906			
071010A	0.98	spec	6	4	0.044	906			
071010B	0.947	spec	> 35.7	2.4	0.005	906		(26) (27) (28)	
071031	2.692	spec	180	5.1	0.005	1612		(29) (4)	
071112C	0.823	spec	15	1.5	0.053	906		(30) (4)	
071122	1.14	spec	68.7	0	0.021	1209			
080319C	1.949	spec	34	5.4	0.012	1209		(32) (4)	
080430	0.767	spec	16.2	4.27	0.006	906		(33) (34)	
080520	1.546	spec	2.8	33	0.037	1209		(35) (4)	
080603B	2.689	spec	60	1.6	0.006	1612		(36) (4)	
080605	1.64	spec	20	6.4	0.061	1209		(37) (4)	
080707	1.232	spec	27.1	4.9	0.045	1209		(38) (4)	
080710	0.845	spec	120	1.51	0.034	906		(39) (4)	
080805	1.504	spec	78	12.1	0.019	1209		(40) (4)	
080916A	0.689	spec	60	7.1	0.009	906		(41) (4)	
080928	1.692	spec	280	4.3	0.03	1209		(42) (4)	
081007	0.53	spec	10	5.4	0.007	906	spec		
081008	1.967	spec	185.5	1.4	0.043	1209		(44) (45)	(b)
081121	2.512	spec	14	3.5	0.023	1612			
090418A	1.608	spec	56	13.9	0.02	1209			
090424	0.544	spec	48	4.71	0.011	906		(48) (49)	
090618	0.54	spec	113.2	2.57	0.04	906	phot		
091127	0.49	spec	7.1	1.31	0.017	906	phot	(51) (52) (53)	(e)
091208B	1.063	spec	14.9	9	0.024	1209			

Table 2.1: The LGRBs imaged by *HST* in this program, with various previously available data. Columns list in order: the LGRBs' burst identifier, the redshift, the source of the redshift (spectroscopy of the afterglow (spec), photometry of the assumed host galaxy (ph(host)) or spectroscopy of the assumed host galaxy (host)), the duration over which 90% of the total gamma-ray fluence was seen, the gamma-ray fluence, the measured column density along the LGRB line sight from the X-ray spectrum (Evans et al., 2009), galactic absorption in the H band (*HST's* F160W filter) (Schlafly & Finkbeiner, 2011), the exposure time of the *HST* image to the nearest second (more distant LGRBs were given longer exposures to reduce non-detections) and whether there was any detection of an associated supernova (either spectroscopically or photometrically). Two of the bursts have either no redshift estimate or an upper limit, as the previously quoted redshifts for these bursts have been withdrawn. References are available in thesis appendix.

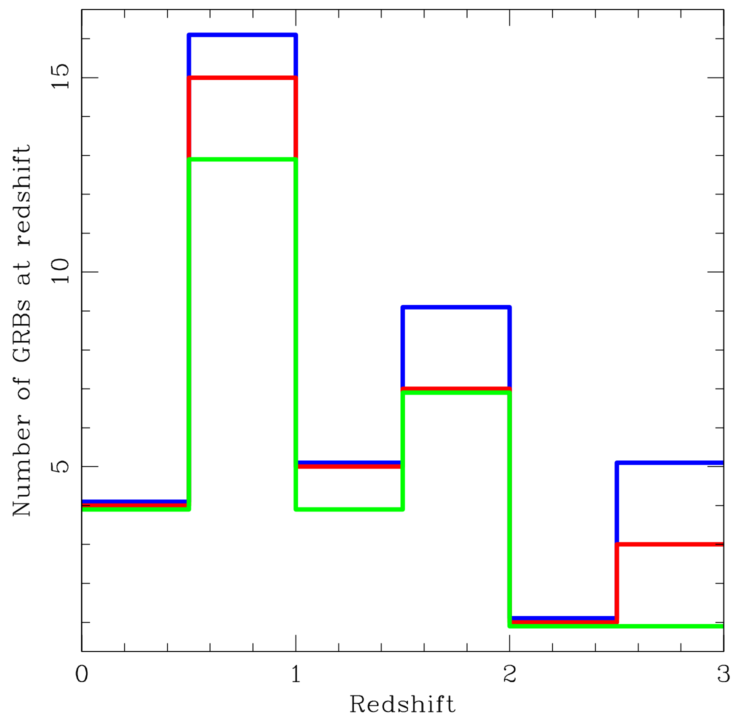

Figure 2.1: A histogram of the redshift distribution of the LGRBs in the sample, in redshift bins of 0.5. The blue uppermost histogram includes all 40 LGRBs in the main sample. The red histogram is limited to only the 35 LGRBs with identified and detected host galaxies. The green histogram is further limited from the red sample to only the 30 bursts with a burst location known to better than an *HST* pixel in accuracy. The shape of the histogram is explained by the increasing volume of visible space as redshift increases (making LGRBs with higher redshifts more common, at low-to-intermediate redshifts such as these) factored against the increased *HST* exposure time for LGRBs at $z > 1$ and again at $z > 2$ (in a snapshot programme where exposures are scheduled in otherwise dead-time between other visits, shorter exposures are significantly more likely to be scheduled).

quality available image of each afterglow was obtained[1] and, if necessary, reduced. Astrometry was performed using IRAF (Tody, 1993), by identifying and centroiding the afterglow and a set of reference stars visible (typically 10 or more) in both images using the “imexam” tool, using the reference stars and “geomap” to calculate the geometric shift from one image to other and then “geoxytran” to overlay the afterglow’s centroided position onto the *HST* image. Positional errors in both the geometric shift and centroiding were converted into *HST* pixels and added in quadrature resulting in a 1-sigma error circle on each *HST* image of the position of the LGRB, which should accurately reflect the uncertainty in the LGRB’s position on the *HST* image. The error generally was dominated by the quality of the afterglow image: poor

[1]Most afterglow images were acquisition images from VLT and Gemini taken prior to spectroscopy, although imaging from *Swift*, *HST*, CTIO Blanco, WHT and NOT were also used

seeing, using smaller telescopes and faint afterglows were the main sources of error. However, in most cases the position of the LGRB was located to within an individual *HST* pixel.

The host galaxy was then located (or a non-detection identified by eye) and aperture photometry was performed using a custom script, either for the host galaxy or a circular aperture with a 5 pixel radius placed over the burst location, giving the magnitude of the host galaxy or an appropriate upper limit. In the case of non-detections this allowed us to ensure that the photometry script did not encounter any three-sigma detections within the area of the burst (double checking the initial human assessment), and provide an upper magnitude limit on the host.

In some cases, the host galaxy appeared to be irregular or part of a merging or interacting system. In order to have self-consistent criteria to decide whether the two galaxies were independent or part of the same system, we used Source Extractor (Bertin & Arnouts, 1996) with a constant set of parameters to identify whether the interacting pair were treated as a single system or two independent sources. All subsequent results, including the host photometry, reflects this identification. Chance alignments are unlikely (typically only $\sim 1\%$ (Cobb & Bailyn, 2008)) so the posibility was ignored for this study, excluding GRB 081007 where an apparently interacting companion of the host galaxy was shown to be a chance alignment of a lower redshift galaxy by absorption lines in the afterglow spectrum. As most of our hosts have spectroscopic redshifts, this further suggests that chance alignments are unlikely as in most cases they would have been detected in the afterglow spectrum when the redshift was obtained.

2.2.3 Astrometry and photometry results

While only 40 LGRBs are included in our main sample and results, 43 fields were imaged in the program. The remaining three were not used: one image (of the site of GRB 060512) was unusuable, as guide star acquisition failed on the *HST* and the image was taken on gyros only, resulting in drifting during the exposure and point sources “streaked” across the sky (in addition, there is likely a nearby foreground galaxy (Fynbo et al., 2009) and some doubt over the redshift), consequently this LGRB is excluded from the remainder of this paper; the quoted redshift of 050803 was from a spectrum of an extended object that at the time was believed to be the host, but on examination of the *HST* data appears to have been a nearby, unrelated galaxy; and the claimed redshift of GRB 070508 was withdrawn after later analysis (Fynbo et al., 2009). For GRBs 050803 and 070508 partial analysis has been performed and is included in the data tables for completeness, but they have not been used in any subsequent stages of analysis.

For the 40 fully analysed images, the host was identified and detected in 35 cases - for the other 5 LGRBs only an upper limit on the host's magnitude can be provided. Of the 35 host galaxy detections, the astrometry was accurate enough to identify the burst location to a particular pixel in 30 hosts.

For five of the bursts with detected hosts, a sub-pixel position on the *HST* image was not possible. For GRB 070521 this was because it was a dark burst, for which no optical afterglow was detected to deep limits (Perley et al., 2009). For GRB 081121 and GRB 050406, the best afterglow images available were taken with the small UVOT telescope on board *Swift*, and only had sufficient resolution to localise the burst to its host. For GRB 051016B, we do not have access to any afterglow imaging of sufficient quality to locate the burst, however using information published in GCN (the Gamma-ray Coordinates Network[2]) reports the host galaxy was confidently identified. For GRB 060912A, the only afterglow image is heavily host contaminated and has poor signal to noise, so while it can be used to easily identify the host by eye it is of insufficient quality to allow subpixel astrometry.

All of the images, with the burst locations or host galaxies marked, are shown in Figures 2.2 and 2.3.

Table 2.2 shows the results of the astrometry and photometry, including details of the afterglow imaging used to perform the relative astrometry. Notes on the table: (a) No afterglow image of sufficient quality available to localise burst, however it can be associated with a particular galaxy using information published in GCN reposts; (b) Blurred image, as *HST* failed to achieve guide star lock during this pointing; (c) Dark burst, photometry is of the probable host identified by Perley et al. (2009), from which the redshift was obtained; (d) This host

[2]http://gcn.gsfc.nasa.gov/

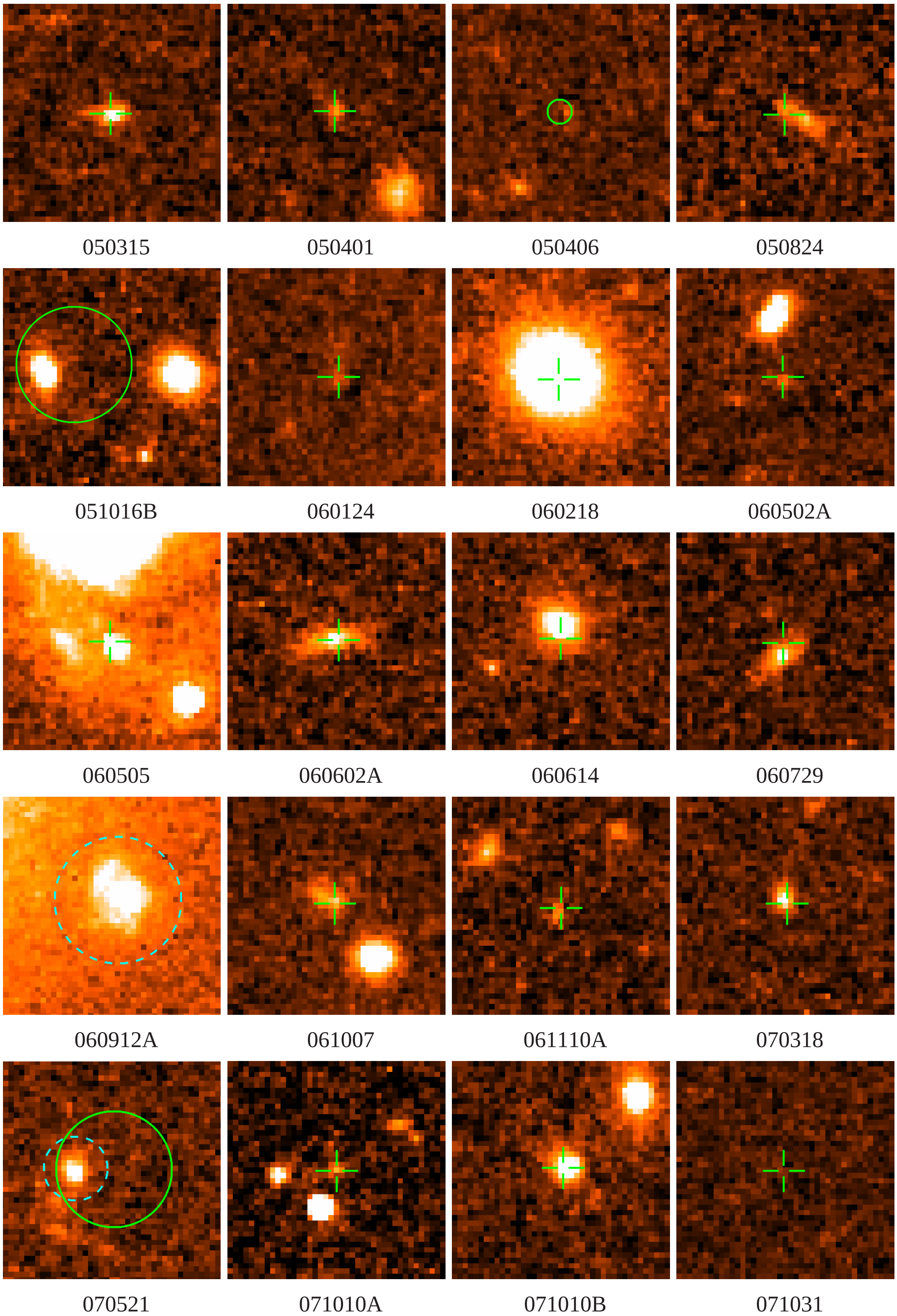

Figure 2.2: The first half of the 40 *HST* images from this program. Each image is labelled with the relevant LGRB's burst identifier. Where the position of the LGRB is known to better than an *HST* pixel ($\sim 0.13''$) the location is indicated with a green cross. For GRB 050406 a green circle indicates the one sigma error circle from our astrometry, in both cases clearly containing the assumed host. For GRBs 051016B and 070521 a green circle indicates the 90% error circle on the enhanced XRT position provided by *Swift*. For GRBs 060912A and 070521 a dashed cyan circle identifies the host galaxy, chosen by visual comparison with a host-contaminated afterglow image and images in (Perley et al., 2009) respectively. The three rejected images are not included. Each image corresponds to a square region on the sky $5.25''$ to a side.

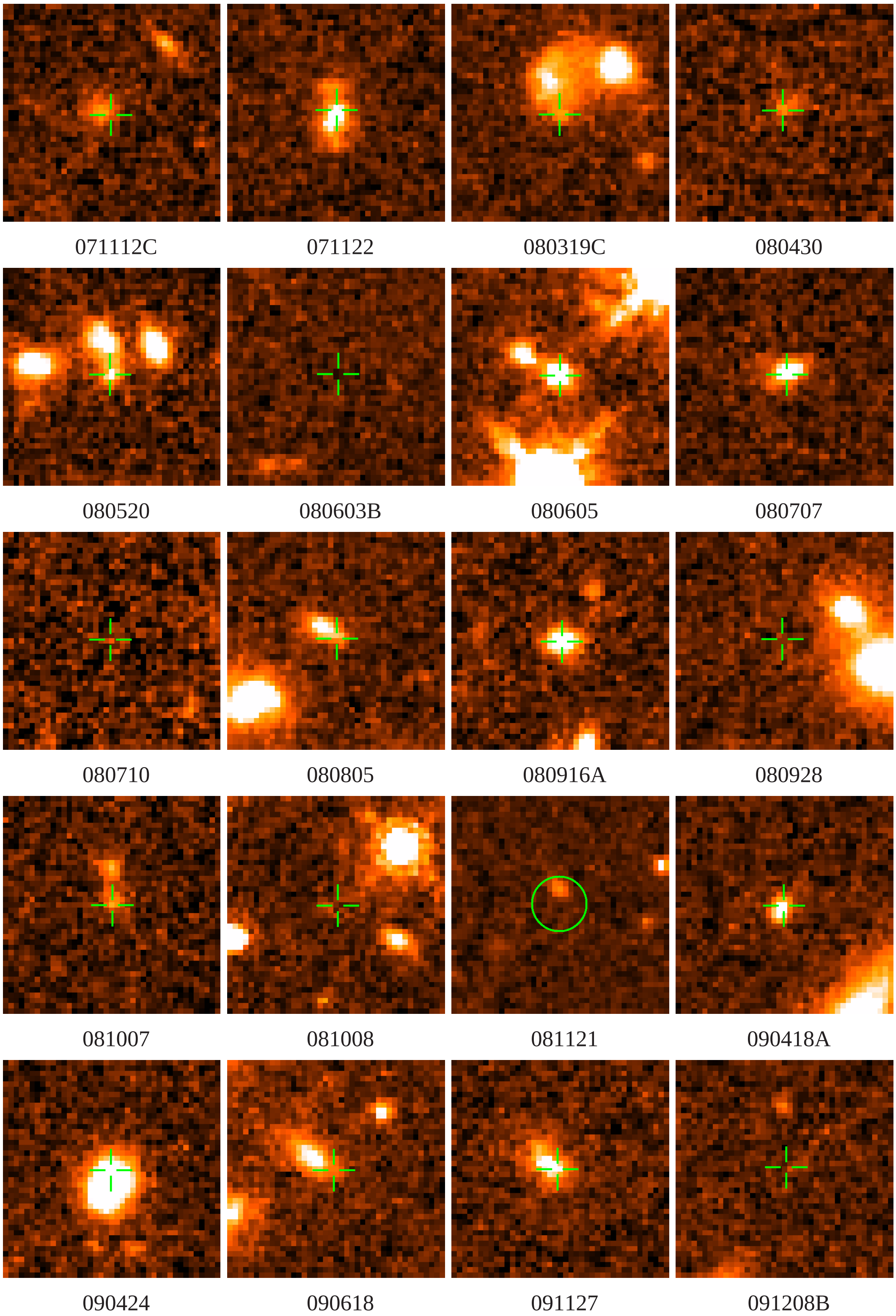

Figure 2.3: The second half of the 40 *HST* images from this program. Each image is labelled with the relevant LGRB's burst identifier. Where the position of the LGRB is known to better than an *HST* pixel ($\sim 0.13''$) the location is indicated with a green cross. For GRB 081121 a green circle indicates the one sigma error circle from our astrometry, clearly containing the assumed host. The three rejected images are not included. Each image corresponds to a square region on the sky $5.25''$ to a side.

galaxy consists of two "knots" which appear to be a merging or interacting system, this is photometry of the entire system as a whole; (e) Burst lies between two relatively bright stars, which may affect the quality of the photometry; (f) This host appears to consist of two interacting galaxies, this is photometry of only the lower galaxy, from which the LGRB originated; (g) Photometry finds a source at the burst location with $4.9\ \sigma$ confidence, however there is no obvious host galaxy here and this position lies under the diffraction spike of a bright star, making this likely a false detection.

2.2.4 Image analysis - burst location and galaxy morphology

Following the methodology laid down in Fruchter et al. (2006), we calculated the "cumulative fraction of host light value" (f-light value) for each LGRB located to better than a pixel in accuracy, with a detected host. For each LGRB satisfying these criteria, we used Source Extractor to select only the host galaxy, then ranked all of the pixels in ascending order of brightness. We then turned this into a cumulative distribution and normalised it to 1, and ascertained the value of the pixel that the LGRB originated from. This is the f-light value for the LGRB, which corresponds to the fraction of total host light in pixels fainter than or equal to the light of the pixel containing the LGRB site. An f-light value of 1 indicates a burst occurring in the brightest pixel of its host galaxy, whereas an f-light value of 0 would indicate a burst happening outside the detectable portion of the galaxy assumed to be its host.

We experimented with a variety of aperture sizes, however they had no effect as long as the entire galaxy was enclosed. Including extra background made no difference as the values of the noise on background *HST* pixels was negligible in comparision to the values of the pixels of the host, so would make no difference to the cumulative distribution which is dominated by the brightest pixels. Furthermore, as the background pixels have both positive and negative values, the background pixels had a tendancy to cancel themselves out within the cumulative distribution. As the distribution used to create the f-light value is dominated by the brightest pixels in the host, this also means that if faint portions of the galaxy are lost into the background there is little effect on the f-light value, as the faintness of that area of the host implies it would have had little effect on the distribution.

GRB	z	Source of astrometry	Delay (hrs)	Position error ($''$)	galaxy mag (AB)	mag error	M_{host} (AB)	Notes
050315	1.949	CTIO Blanco	11.3	0.053	23.806	0.046	-22.157	
050401	2.898	VLT	14.7	0.079	25.18	0.133	-21.857	
050406	2.7	*Swift*	0.1	0.289	26.197	0.195	-20.609	
050803	?	n/a	n/a	n/a	$>$ 25.470	n/a	n/a	
050824	0.828	VLT	9.5	0.081	23.894	0.088	-19.746	
051016B	0.936	n/a	n/a	n/a	22.411	0.021	-21.557	(a)
060124	2.3	WHT	148	0.017	24.84	0.178	-21.648	
060218	0.033	Gemini South	68.7	0.018	19.628	0.031	-16.297	
060502A	1.503	Gemini North	4.8	0.024	25.649	0.175	-19.611	
060505	0.089	Gemini South	26.6	0.023	17.619	0.006	-20.421	
060512	2.1	n/a	n/a	n/a	n/a	n/a	n/a	(b)
060602A	0.787	NOT	0.3	0.048	22.913	0.081	-20.573	
060614	0.126	VLT	20.9	0.035	22.086	0.041	-16.747	
060729	0.543	*HST*	217.4	0.008	23.377	0.103	-19.133	
060912A	0.937	n/a	n/a	n/a	21.657	0.149	-22.329	
061007	1.262	VLT	14.9	0.066	24.079	0.044	-20.68	
061110A	0.758	VLT	14.4	0.045	25.217	0.154	-18.233	
070318	0.84	VLT	16.4	0.057	24.32	0.044	-19.321	
070508	$<$ 3	VLT	3.8	0.048	22.964	0.062	-20.747	
070521	1.35	n/a	n/a	n/a	23.39	0.035	-21.56	(c)
071010A	0.98	VLT	21.9	0.028	25.265	0.169	-18.887	
071010B	0.947	Gemini North	17.7	0.038	22.781	0.022	-21.19	
071031	2.692	VLT	0.9	0.05	$>$ 26.118	n/a	$>$ -20.670	
071112C	0.823	VLT	8.8	0.033	23.952	0.08	-19.748	
071122	1.14	Gemini North	3	0.036	22.728	0.038	-21.784	
080319C	1.949	Gemini North	2.3	0.023	22.287	0.028	-23.655	
080430	0.767	NOT	1.3	0.028	24.74	0.112	-18.664	
080520	1.546	VLT	7.3	0.061	22.442	0.03	-22.929	(d)
080603B	2.689	NOT	1.9	0.087	$>$ 26.046	n/a	$>$ -20.741	
080605	1.64	VLT	1.7	0.052	22.037	0.027	-23.55	(d), (e)
080707	1.232	VLT	0.9	0.095	22.987	0.038	-21.784	
080710	0.845	Gemini North	4.1	0.028	$>$ 25.507	n/a	$>$ -18.222	
080805	1.504	VLT	0.8	0.053	23.352	0.037	-21.909	
080916A	0.689	VLT	18.4	0.072	22.817	0.022	-20.306	
080928	1.692	VLT	15.5	0.061	$>$ 25.904	0.378	$>$ -19.697	
081007	0.53	Gemini South	1	0.038	24.938	0.079	-17.481	(f)
081008	1.967	Gemini South	3.9	0.018	$>$ 25.349	n/a	$>$ -20.686	(g)
081121	2.512	*Swift*	0.8	0.658	25.042	0.092	-21.694	
090418A	1.608	Gemini North	2.5	0.075	23.811	0.039	-21.629	
090424	0.544	Gemini South	11.5	0.021	21.316	0.012	-21.184	
090618	0.54	WHT	16.9	0.051	22.668	0.042	-19.876	
091127	0.49	Gemini North	9.9	0.045	22.811	0.041	-19.427	
091208B	1.063	Gemini North	1.2	0.019	25.701	0.333	-18.627	

Table 2.2: The astrometric and photometric results for the LGRB hosts. Columns list in order: the LGRBs' burst identifier, the redshift, the telescope used to provide the afterglow image for astrometry, how soon after the LGRB the afterglow image used was taken, the total error in the astrometry in arcseconds, the measured magnitude of the host galaxy or an upper limit for non-detections (no correction made for galactic extinction), the error on the magnitude for detected host galaxies and the absolute magnitude of the LGRB host galaxy M_{host} (without K-correction to account taken for the differing rest-frame wavelengths, but corrected for galactic extinction using the A_H values from Schlafly & Finkbeiner (2011) as published in Table 2.1). For LGRBs with slightly revised redshifts, such as those included in Fynbo et al. (2009) or Hjorth et al. (2012), the most accurate redshift is quoted but the original redshift source is also referenced.

Morphology was quantified using the collection of methods laid out in Conselice (2003) to calculate the concentration (C), asymmetry (A) and clumpiness (S) of the light distribution of the host galaxies, as has been used to quantify galaxy morphology at high redshift for some time (e.g. Abraham et al. (1996)).

The concentration (C) is calculated by Conselice (2003) using the method previously utilised by Bershady et al. (2000), which defines it as:

$$C = log(r_{80}/r_{20})$$

where r_{80} and r_{20} are the radii that contain 80% and 20% of the galaxy's light, respectively. Galaxies with steeper light profiles, such as elliptical galaxies, will therefore have higher values for C.

The asymmetry (A) is determined by rotating an image of the galaxy by 180° about the galactic centre and subtracting this from the unrotated image. The pixel values in the resultant image are normalised and background corrected and then used to calculate the asymmetry value Conselice et al. (2000); Conselice (2003):

$$A = min\frac{\Sigma|I_0 - I_\phi|}{\Sigma|I_0|} - min\frac{\Sigma|B_0 - B_\phi|}{\Sigma|I_0|}$$

where I_0 and I_ϕ are pixel intensities of the original and rotated images, respectively, and B_0 and B_ϕ represent the background regions used to account for background noise in the original and rotated images, respectively. A perfectly symmetrical galaxy will give an A value of 0, while features such as bright star-forming regions and major or minor mergers will cause asymmetries in the galaxy that will be reflected by the value of A.

The clumpiness (S) is determined as discussed in Conselice (2003). However, it is a complex calculation, and as will be later discussed in Section 2.3 the resolution of the vast majority of our images turns out to be insufficient to measure S, so the value is not used in the data analysis and the methodology is not reprinted here. Errors are calculated based on the signal-to-noise ratio Conselice et al. (2000).

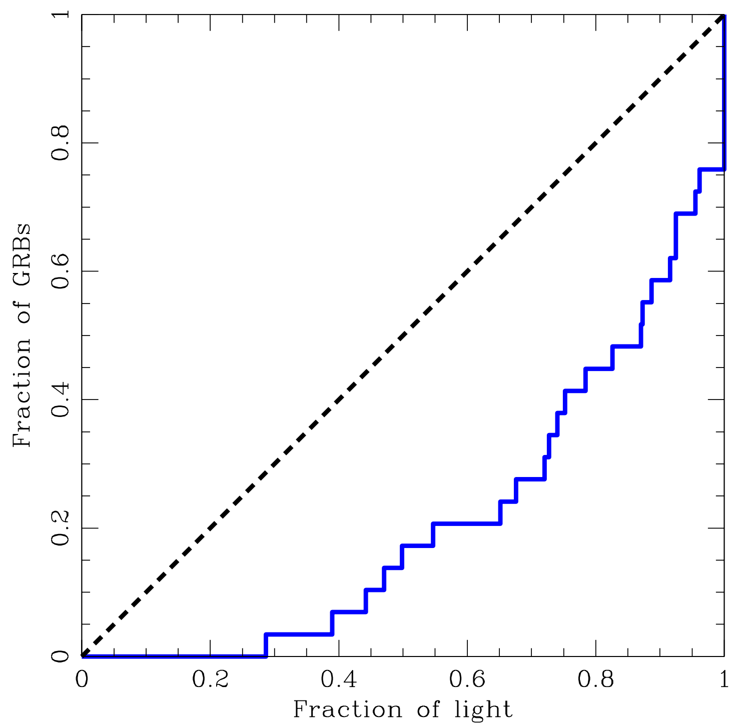

Figure 2.4: A cumulative histogram of the f-light values, showing the cumulative fraction of LGRBs found at a given fraction of the host's brightness. A short-dashed line from the origin to (1,1) indicates the distribution expected if LGRBs merely trace the light on their host - as the distributions are all rightward of this line, the data indicate that LGRBs are more likely to occur in the brightest regions of their hosts than randomly selected stars.

2.2.5 Burst location and galaxy morphology results

The f-light values calculated in Section 2.2.4 are plotted for all bursts as a cumulative distribution (again normalised to 1) in Figure 2.4. If LGRBs traced star formation in their host galaxies then the probability of a burst occurring in a particular pixel would be proportional to the brightness of that pixel (the distribution observed for core-collapse SNe in optical bands), causing the distribution to follow a straight line from (0,0) to (1,1), as represented by the dashed line in Figure 2.4. However, the observed distribution shown indicates that LGRBs are far more likely to be located in the brightest pixels of their hosts in the NIR, echoing the results that Fruchter et al. (2006) found in the optical, and implying they are biased towards the brightest star forming regions.

In Figure 2.5 the same data are presented, but this time divided into three redshift bins of $z < 0.75$, $0.75 \leq z < 1.5$ and $z \geq 1.5$. At higher redshifts, the LGRBs are more concentrated

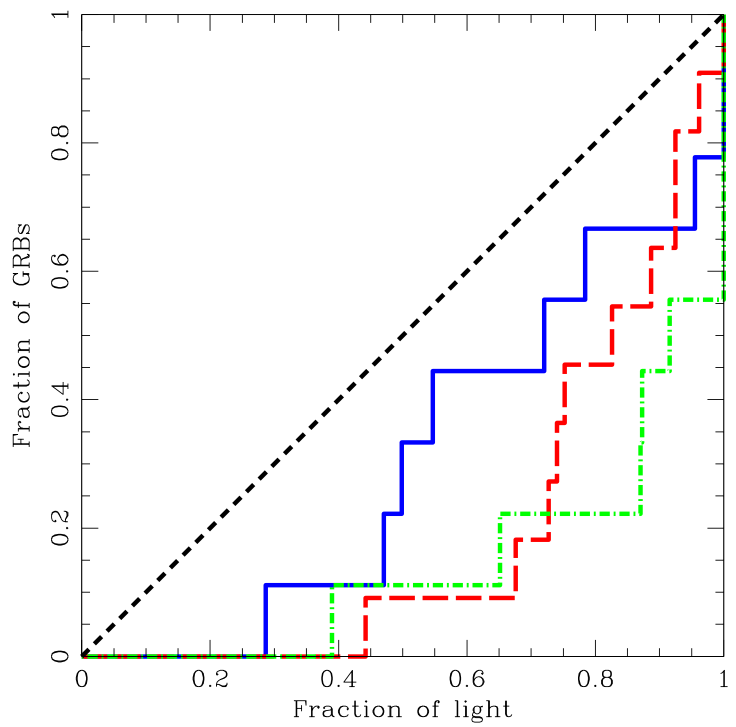

Figure 2.5: The same data as in Figure 2.4, but split up into three redshift bins: $z < 0.75$ in blue (solid line), $0.75 \leq z < 1.5$ in red (long dashed line) and $z \geq 1.5$ in green (line with alternating dashes and dots). As in Figure 2.4 there is a short-dashed line indicating the distribution expected if LGRBs trace the light on their host. There is a some indication that higher redshift LGRBs tend to be more concentrated on the brightest regions of their hosts.

on the light of their host galaxies than at lower redshifts, although at all redshifts they show a propensity towards their hosts' brightest regions. As the f-light value is dominated by the brightest pixels of the host galaxy, there should be negligibal effect due to fainter hosts at higher redshifts. Likewise one expects negligable effects from higher redshift objects taking up fewer pixels, as it should not effect the shape of the f-light distribution. Whether this trend can be entirely attributed to the changing restframe wavelength of the hosts (as the redshift increases, the restframe wavelength pushes into the optical where star formation and young star-forming regions should be more pronounced) or is also due in part to a redshift evolution is not clear, but could be examined further in future by comparing the higher redshift LGRB hosts with an *HST* imaged comparison sample of lower redshift LGRBs hosts in optical wavelengths, or more conclusively by a multi-wavelength survey.

In Figure 2.6 the morphological quantities C and A are plotted against each other, compared to the results in the optical from Conselice et al., 2005. Both samples span the same $0 < z < 3$ redshift range, although the sample from Conselice et al., 2005 contains several burts of unknown redshift and uses *HST* data from other previous surveys, thus is subject to any selection biases that went into them and uses several different instruments (STIS, WFPC2, and ACS). In future studies a multiwavelength approach would be preferable, should sufficient telescope time be available, however for the purposes of this study the sample from Conselice et al., 2005 suffices as an adequate comparison sample.

The data suggest that near-infrared imaged LGRBs appear less centrally concentrated, and perhaps slightly less asymmetric, leading to more of the hosts falling in the “spirals” category of the plot. The two samples should be comparable in selection methods, so the difference is unlikely to be due to selection biases and represent an underlying difference in the apparently morphologies of LGRB host galaxies in different rest-frame wavelengths. The negative A values (excluded from the figure in line with Conselice et al. (2005)) are likely due to the relatively small angular size of our host galaxies in detector pixels, unfortunately this is an unavoidable limitation until larger observatories become available in the future.

Tables 2.3 and 2.4 show the results for the burst locations and the morphologies of the host galaxies.

2.2.6 LGRB host galaxies as cosmic star formation rate tracers

The cosmic star formation rate (SFR) is observed to peak at around $z \sim 2$ (e.g. Madau et al. (1998), Hopkins & Beacom (2006)). However, it is not clear what the dominant source(s) of this star formation are - major mergers, or less disruptive sources such as minor mergers and cold accretion (see e.g. Kaviraj et al. (2013) and citations therein).

While LGRBs are believed to preferentially occur in lower metallicity environments, at higher redshifts, where average metallicities were substantially lower, it is not unreasonable to suggest that they may act as relatively unbiased selectors of galaxies, i.e. that at higher redshifts the probability of a galaxy containing a LGRB is (roughly) proportional to its SFR. If this were the case, then the fraction of LGRB host galaxies undergoing major mergers should be roughly equal to the fraction of the star formation budget contained within merging galaxies

GRB	z	Host Found?	ϵ	Position error (kpc)	Burst offset (kpc)	r_{80} (kpc)	Cumulative f-light position	Notes
050315	1.949	Yes	0.348	0.338	0.233	3.81	1	
050401	2.898	Yes	0.453	0.501	0.72	3.809	1	
050406	2.7	Yes	0.378	2.326	1.985	2.483	n/a	
050803	?	No	n/a	n/a	n/a	n/a	n/a	
050824	0.828	Yes	0.556	0.689	3.404	4.695	0.826	
051016B	0.936	Yes	0.317	n/a	n/a	3.947	n/a	
060124	2.3	Yes	0.236	0.127	0.494	3.548	0.916	
060218	0.033	Yes	0.135	0.153	0.115	0.842	0.955	
060502A	1.503	Yes	0.368	0.17	0.658	2.797	0.873	
060505	0.089	Yes	0.343	0.194	6.797	6.196	0.498	
060512	2.1	n/a	n/a	n/a	n/a	n/a	n/a	
060602A	0.787	Yes	0.564	0.3	1.258	5.814	0.925	
060614	0.126	Yes	0.049	0.217	0.835	1.853	0.471	
060729	0.543	Yes	0.506	0.064	2.096	3.642	0.286	
060912A	0.937	Yes	0.253	n/a	n/a	n/a	n/a	(a)
061007	1.262	Yes	0.184	0.562	2.055	5.257	0.925	
061110A	0.758	Yes	0.325	0.286	0.894	2.715	0.442	
070318	0.84	Yes	0.219	0.358	1.333	2.591	0.752	
070508	< 3	Yes	0.373	0.288	2.539	8.313	0.767	
070521	1.35	Yes	0.383	n/a	n/a	5.93	n/a	
071010A	0.98	Yes	0.265	0.23	0.368	2.998	1	
071010B	0.947	Yes	0.183	0.302	1.108	5.377	0.676	
071031	2.692	No	n/a	0.404	n/a	n/a	n/a	
071112C	0.823	Yes	0.287	0.254	2.431	8.257	0.74	
071122	1.14	Yes	0.409	0.299	0.926	5.946	0.961	
080319C	1.949	Yes	0.334	0.193	7.087	7.763	0.652	
080430	0.767	Yes	0.229	0.208	1.29	5.004	0.887	
080520	1.546	Yes	0.38	0.389	4.044	4.725	0.87	
080603B	2.689	No	n/a	0.704	n/a	n/a	n/a	
080605	1.64	Yes	0.63	0.441	2.94	6.939	1	
080707	1.232	Yes	0.335	0.797	0.68	4.436	0.727	
080710	0.845	No	n/a	0.212	n/a	n/a	n/a	
080805	1.504	Yes	0.337	0.45	3.572	7.286	0.39	
080916A	0.689	Yes	0.168	0.51	0.135	3.145	1	
080928	1.692	No	n/a	0.522	n/a	n/a	n/a	
081007	0.53	Yes	0.112	0.236	0.844	3.225	1	
081008	1.967	No	n/a	0.157	n/a	n/a	n/a	
081121	2.512	Yes	0.285	5.384	n/a	2.866	n/a	
090418A	1.608	Yes	0.164	0.641	0.707	5.017	1	
090424	0.544	Yes	0.205	0.13	2.278	4.405	0.72	
090618	0.54	Yes	0.205	0.324	5.244	7.52	0.547	
091127	0.49	Yes	0.283	0.272	2.098	4.554	0.784	
091208B	1.063	Yes	n/a	0.153	n/a	n/a	n/a	

Table 2.3: Measured burst location and host galaxy properties. Columns list in order: the LGRBs' burst identifier, the redshift, whether or not the host galaxy was detected in the *HST* image, the host galaxy's ellipticity ϵ, the accuracy to which the bursts location upon the host is known in kpc, the distance of the LGRBs location to the optical centre of the galaxy as measured by Source Extractor, the radius containing 80% of the Petrosian flux, the cumulative brightness of the pixel containing the LGRB normalised to 1 with respect to the brightest pixel in the galaxy (using the method of Fruchter et al. (2006)). Notes: (a) r_{80} value is significantly overestimated due to light from a nearby low-z galaxy.

GRB	z	Host Found?	C	E(C)	A	E(A)	S	E(S)
050315	1.949	Yes	2.444	0.311	0.128	0.031	0	0
050401	2.898	Yes	1.991	0.349	0.056	0.091	0	0
050406	2.7	Yes	1.204	0.431	0.048	0.117	0	0
050803	?	No	n/a	n/a	n/a	n/a	n/a	n/a
050824	0.828	Yes	2.649	0.259	0.058	0.062	0	0
051016B	0.936	Yes	2.47	0.314	0.309	0.011	0	0
060124	2.3	Yes	1.814	0.32	-0.11	0.151	0	0
060218	0.033	Yes	3.152	0.194	0.174	0.004	0	0
060502A	1.503	Yes	1.193	0.434	-0.16	0.089	0	0
060505	0.089	Yes	3.473	0.087	0.167	0.003	0.109	0.004
060512	2.1	n/a	n/a	n/a	n/a	n/a	n/a	n/a
060602A	0.787	Yes	2.974	0.242	0.256	0.057	0	0
060614	0.126	Yes	2.939	0.24	0.019	0.016	0	0
060729	0.543	Yes	2.376	0.295	0.038	0.044	0	0
060912A	0.937	Yes	3.226	0.111	0.491	0.058	0.47	0.043
061007	1.262	Yes	2.644	0.259	0.152	0.058	0	0
061110A	0.758	Yes	1.932	0.356	-0.24	0.064	0	0
070318	0.84	Yes	1.914	0.361	0.017	0.032	0	0
070508	< 3	Yes	3.163	0.194	0.292	0.077	0	0
070521	1.35	Yes	3.174	0.268	0.297	0.051	0	0
071010A	0.98	Yes	1.208	0.434	-0.01	0.004	0	0
071010B	0.947	Yes	2.463	0.305	0.29	0.017	0	0
071031	2.692	No	n/a	n/a	n/a	n/a	n/a	n/a
071112C	0.823	Yes	2.945	0.241	0.087	0.09	0	0
071122	1.14	Yes	2.95	0.243	0.111	0.03	0	0
080319C	1.949	Yes	2.437	0.189	0.351	0.022	0	0
080430	0.767	Yes	3.227	0.23	-0.04	0.185	1.06	0.092
080520	1.546	Yes	2.437	0.302	0.054	0.012	0	0
080603B	2.689	No	n/a	n/a	n/a	n/a	n/a	n/a
080605	1.64	Yes	2.939	0.294	0.118	0.009	0	0
080707	1.232	Yes	2.446	0.305	0.205	0.022	0	0
080710	0.845	No	n/a	n/a	n/a	n/a	n/a	n/a
080805	1.504	Yes	2.415	0.298	0.13	0.03	0	0
080916A	0.689	Yes	2.441	0.311	0.105	0.015	0	0
080928	1.692	No	n/a	n/a	n/a	n/a	n/a	n/a
081007	0.53	Yes	2.413	0.304	0.235	0.087	0	0
081008	1.967	No	n/a	n/a	n/a	n/a	n/a	n/a
081121	2.512	Yes	1.933	0.359	0.015	0.052	0	0
090418A	1.608	Yes	1.958	0.343	0.175	0.022	0	0
090424	0.544	Yes	2.539	0.245	0.204	0.009	0	0
090618	0.54	Yes	3.312	0.207	0.127	0.051	0	0
091127	0.49	Yes	2.932	0.239	0.14	0.032	0	0
091208B	1.063	Yes	n/a	n/a	n/a	n/a	n/a	n/a

Table 2.4: Measured host galaxy morphology. Columns list in order: the host galaxy's concentration (C), asymmetry (A) and clumpiness (S) with respective errors, using the method of Conselice (2003) as further discussed in the text.

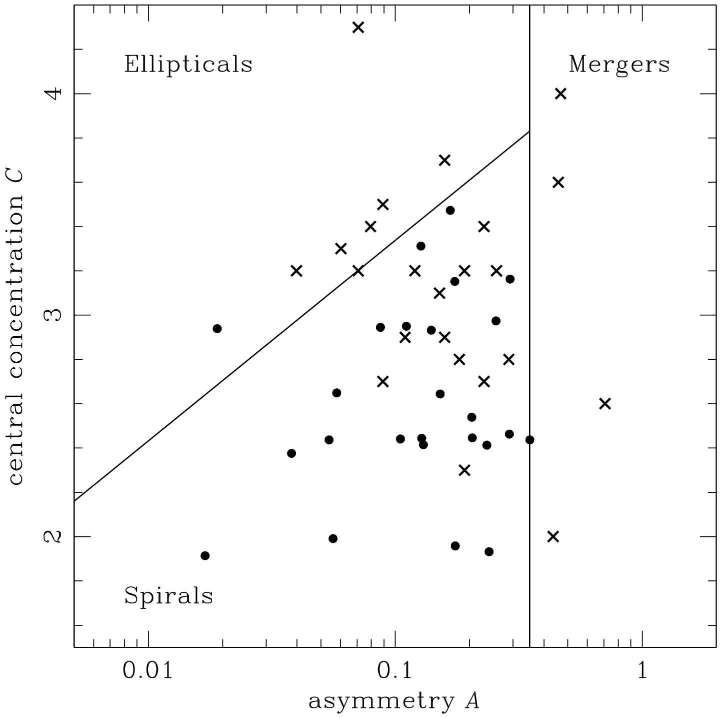

Figure 2.6: The morphology results from this paper (filled circles) plotted with the results from Conselice et al. (2005) (crosses), which were taken in the optical. Only those host galaxies from Conselice et al. (2005) with known redshifts $z < 3$ are plotted, for fair comparison. Five hosts from this sample and one from Conselice et al. (2005) have negative values for A therefore do not appear in this plot. Also shown are the three regions proposed in Conselice et al. (2005) which roughly define different host morphologies based on their C and A values. Error bars are omitted for clarity, but are published in Table 2.4.

at these redshifts.

To test this, we created a subsample of all the LGRB host galaxies in our sample with redshifts in the range $1.5 < z < 3$, which corresponds to 12 LGRB host galaxies and 3 non-detections. We then use the visual classification system of Kaviraj et al. (2013) to identify any hosts undergoing major mergers, for which we identify two systems - the host galaxies of GRBs 080520 and 080605. This therefore corresponds to 2/12 ($17 \pm 11\%$) of the LGRBs in our subsample being in systems undergoing major mergers.

This value is similar to that of $27 \pm 8\%$ found by Kaviraj et al. (2013), however there are several potential biases involved. The most obvious is that Kaviraj et al. (2013) restrict themselves to galaxies with observed magnitudes in the H band of less than 24.2, which corresponds at $z = 2$ to an absolute magnitude of $\lesssim -21.8$. Very few of the host galaxies in our sample are this bright, and the majority are significantly fainter, so we are probing slightly different galaxy populations. This is compounded by the fact that their fields are significantly deeper, meaning that the disturbed morphologies used to identify merging systems are more easily visible for their sample of galaxies.

It is also worth briefly noting the case of GRB 080319C. On visual inspection of Figure 2.3 it would appear that the host galaxy is interacting with another galaxy of similar size. However, spectroscopy showed that this galaxy is in fact a foreground galaxy that happens to lie almost on top of the host galaxy on the sky. While this could be a potential source of contamination, it should be a relatively rare scenario (typically only $\sim 1\%$ (Cobb & Bailyn, 2008), see discussion in Section 2.2.2), and wouldn't appear in the sample of Kaviraj et al. (2013) at all as they have redshifts for all their galaxies.

However, one can note that while only 12 of the 15 galaxies in the subsample are detected, the upper limits on the absolute magnitudes of the 3 undetected hosts allow us to say that they are all at least two magnitudes fainter than the lower limit of the sample of Kaviraj et al. (2013). If one defines major mergers as not only mergers of galaxies of similar mass, but of *massive galaxies* of similar mass, then the non-detection of the host is in itself sufficient to define the host as not undergoing a major merger (while the validity of the definition may be debatable, it allows us to compare our LGRB selected galaxy survey with more tradition galaxy surveys). This then leaves us with only 2/15 ($13 \pm 9\%$) of our sample undergoing major mergers, below the lower limit of Kaviraj et al. (2013). Furthermore, Kaviraj et al. (2013) go on to point out that much of the star formation in merging galaxies is unrelated to the merger event, so estimate that by multiplying their value of $\sim 27\%$ by 1.2/2.2 (their estimate of the fraction of star formation that is directly caused by the merger) they will get a value of $\sim 15\%$, i.e. implying that while $\sim 27\%$ of cosmic star formation happens in galaxies undergoing major mergers only $\sim 15\%$ is *due* to major mergers. Following the same logic, our values of $\sim 17\%$ and $\sim 13\%$ of star formation in galaxies undergoing major mergers correspond respectively to $\sim 9\%$ and $\sim 7\%$ of the cosmic SFR being due to major mergers.

This strongly implies that if LGRBs are a fair tracer of star formation at $z \sim 2$ then the vast majority of the cosmic SFR is not from massive galaxies undergoing major mergers, but from less disruptive sources of star formation (e.g. minor mergers or cold accretion) and happens in galaxies that are on average less luminous than the massive galaxies typically studied in surveys at higher redshifts. While not a conclusive result, this highlights the power of LGRBs are probes at higher redshifts, as a the burst provides *a priori* knowledge of the location of the host galaxies, allowing non-detections to be folded into the sample and the faintest end of the galaxy luminosity function to be included, which is typically missed in larger field galaxy surveys.

2.3 Discussion

One result of this work is to show that the previously assumed redshift of GRB 050803 from Bloom et al. (2005) is in fact the redshift of a spatially proximate foreground galaxy. Figure 2.7 shows that the extended object from which the redshift was obtained is a significant distance from the 90% error circle from *Swift's* enhanced XRT position, and furthermore that there is a probable detection of a host within the error circle.

Figure 2.8 shows the absolute magnitude of the LGRB host galaxies plotted against their redshifts, including non-detections as upper limits. It indicates that LGRBs at higher redshifts are typically located in brighter galaxies than more recent bursts. This effect could be caused, at least in part, by the change in rest-frame over the width of the sample - while for the lower redshift bursts the imaging was restframe near infra-red, for the higher redshift bursts were imaged in restframe optical bands where young, massive stars will contribute more light. However, the result may well also be contributed to by the overall increasing metallicity of the Universe over time - if LGRBs require environments with lower metallicity (but active star formation), then at higher redshifts where overall metallicity was lower they will likely trace star formation, but as the redshift drops and metallicities increase they will increasingly move towards smaller galaxies where low metallicity, high star formation rate environments still exist. This could also be caused in part by cosmic downsizing (the observed trend of cosmic star formation being more biased towards larger galaxies at higher redshifts). Our selection criteria may also play a part, as larger, denser host galaxies may aid spectroscopic redshift

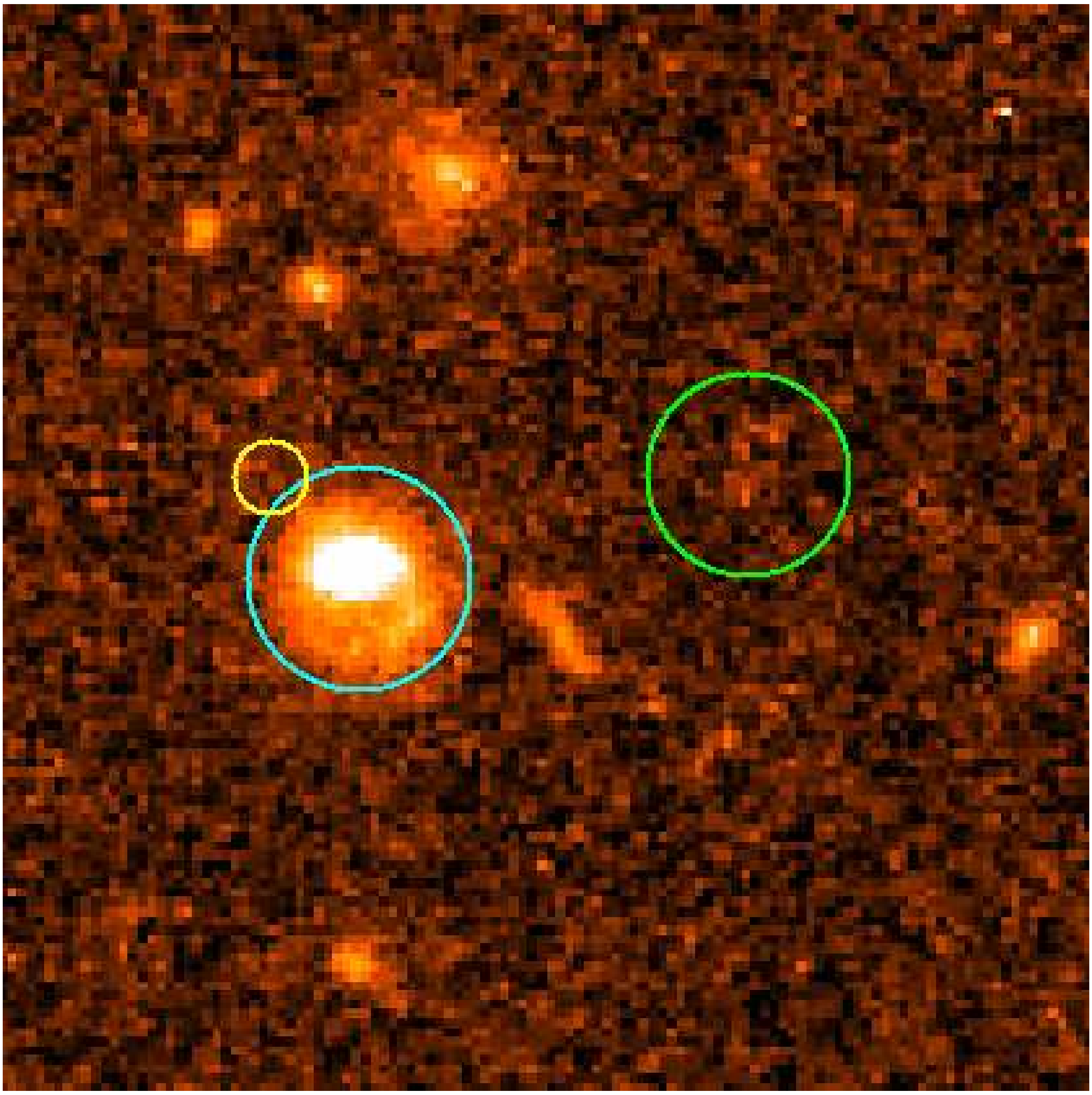

Figure 2.7: The *HST* image of the field of GRB 050803. The green circle to the right of the image shows the enhanced XRT position (90% error circle) of the LGRB as detected by *Swift*. The small yellow circle shows the position and error quoted by Berger et al. (2005a) of the sole source they detected, which they describe as extended. The galaxy circled in cyan below is presumably this source and the object that Bloom et al. (2005) obtained a redshift for of $z = 0.422$. However, this source is significantly outside the enhanced XRT error circle, and furthermore there is a faint source detected within the XRT error circle at a significance of 2.88σ, strongly implying that the redshift 0.422 galaxy is not the host of GRB 050803. The image is $15''$ to a side.

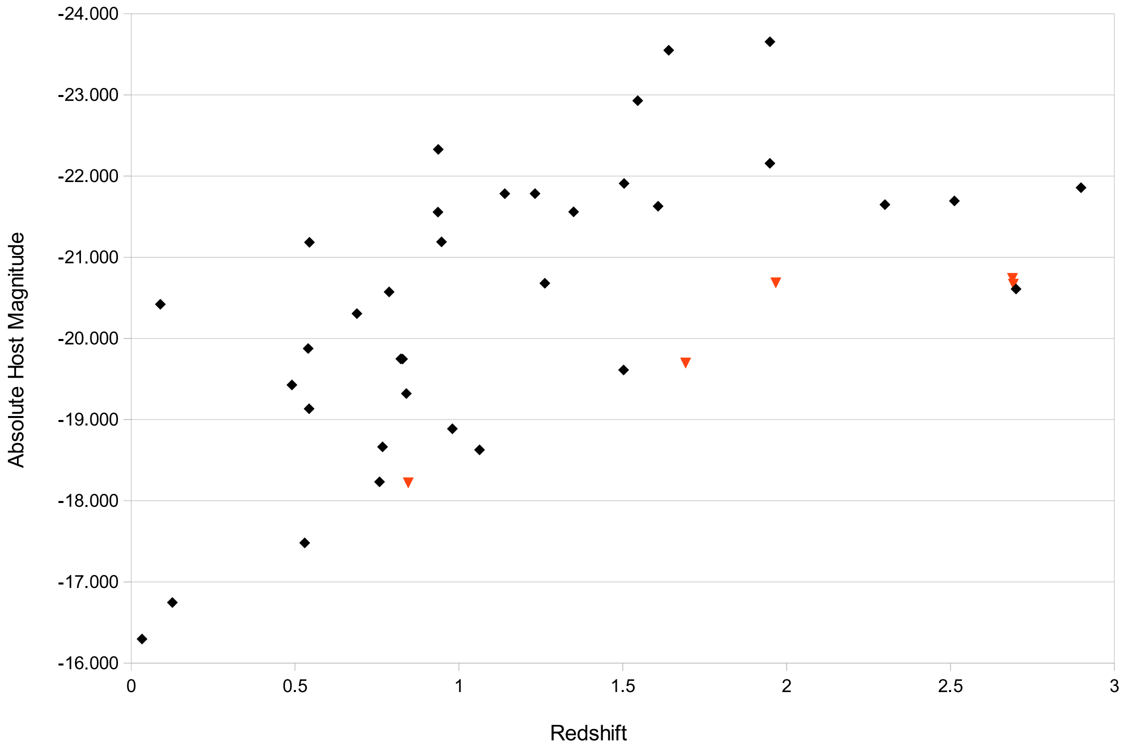

Figure 2.8: LGBR host galaxy absolute magnitudes plotted against their redshifts. Black diamonds indicate detected LGRB host galaxies, red triangles indicate the upper limits from the five non-detections. Faint or dusty galaxies may result in less bright optical afterglows, creating a selection effect towards brighter hosts recieving redshift measurements (a requirement for inclusion in our survey). Magnitude errors are omitted for clarity, however they are published in Table 2.2.

measurements and subtly bias the sample.

During the measurement of the morphology it became apparent that, excluding the very lowest redshift sources, our hosts were too small with respect to the image resolution to resolve sufficient structure to measure the clumpiness value S, giving in most cases a zero value. This still leaves us with two parameters (the concentration C and the asymmetry A) with which to describe the host morphologies, in addition to physical scale of the hosts (as represented by the value r_{80}), which still allows us to compare the hosts to other galaxy samples in the future. There will be some effect on our sample from losing the faint edges of galaxies, however the effect is lessened due using a wavelength less dominated by bright starforming regions, although at higher redshifts as we move closer to rest-frame UV this benefit is lessened somewhat. Furthermore, the small angular size of the galaxies relative to the pixel scale of *HST* limits the method, however it still allows for comparative morphologies to be examined and an idea of the underlying morphologies of these hosts.

By comparing the morphological values C and A of the infra-red imaged LGRB host galaxy sample from this paper with those of an optically imaged sample from Conselice et al. (2005), we find hints that LGRB hosts appear less centrally concentrated and perhaps less asymmetric in the near-infra red, and thus appear more like typical spiral galaxies. As LGRBs are associated with the deaths of massive stars, and thus strongly associated with star formation, this might be explained by the bright star-forming regions LGRBs are born in dominating the light of their hosts in the optical, whereas in the infra-red the light is less dominated by these bright, young stars and thus the "true" galaxy morphology is more visible.

Full interpretation of these results requires their comparison to other samples. In a forthcoming paper we will compare the data for LGRBs gathered here to samples of SNe hosting galaxies and field galaxies, in order to better understand what differentiates LGRB hosting galaxies. These differences should give valuable clues as to the environments required for the creation of LGRBs.

2.4 Conclusions

Understanding the environments in which LGRBs typically form is a crucial route to understanding LGRBs themselves. In this work, we have presented the first large sample of *Swift* detected LGRB host galaxies imaged with *HST* in the infra-red: 40 images of the locations of LGRBs with reported redshifts $z < 3$ (plus three images which were rejected for the majority of the analysis in this paper). These yielded 35 host detections and 5 non-detections, with astrometry capable of identifying the burst location to within an *HST* pixel ($\sim 0.13''$) in 30 of the detected hosts.

We show that the probability of LGRBs occurring in the brightest regions of their host galaxies viewed in the infra-red is similar to that found by Fruchter et al. (2006) in the optical. In our sample we used the H band filter on *HST* centred at 1536.9nm, which at $z = 1$ corresponds approximately to rest-frame SDSS i (near infra-red), at $z = 2$ corresponds approximately to rest-frame SDSS g (green) and at $z = 3$ corresponds approximately to rest-frame SDSS u (ultra-violet). Therefore, for the majority of our sample we are observing rest-frame near infra-red to red light (see the distribution of bursts by redshift in our sample in Figure 2.1), whereas the sample from Fruchter et al. (2006) was imaged in several filters mostly around 585nm (approximately V band), which already corresponds to rest-frame ultraviolet at $z \approx 0.5$. This implies that even with the dominance of light from the youngest star forming regions reduced, the trend holds. Further work will be necessary to ascertain whether this is implying that LGRBs are more likely in the centres of their host galaxies. Clearly, however, we are still probing a large range of rest-frame wavelengths - a multi-wavelength survey or a survey over a small redshift range would be better able to untangle any effects from this.

In addition to the f-light values as originally measured in Fruchter et al. (2006), we have also gathered photometry of those hosts, and gathered a variety of measures of host morphology. These data can only be well interpreted with a comparison sample, so future work is required to gather this sample in order to understand how the morphologies of LGRB hosting galaxies differ from other galaxy populations. Figure 2.5 seems to hint that the f-light might be significantly effected by wavelength, however a multi-wavelength study is needed to confirm the effect and exclude other possibilities, such as a fundamental change in LGRB locations on their hosts with redshift.

The LGRBs used in this sample were pseudo-randomly selected by the *HST* snapshot program from a larger catalogue of possible targets, which were selected on the dual criteria of *Swift* detected LGRBs with known redshifts < 3. This biases the sample towards the hosts of the LGRBs with the brightest afterglows, as these are the LGRBs for which redshifts are typically obtained. Future work might aim to eliminate this bias, however to do so would require a sample of LGRB targets where the redshift has been gathered regardless of the brightness and longevity of the afterglow, i.e. by spectroscopy of the presumptive host galaxy in cases where afterglow spectroscopy has proven impossible. The optically unbiased[3] GRB host (TOUGH) survey (Hjorth et al., 2012) would be a candidate sample, however even this survey has only obtained redshifts for 77% of its targets. Furthermore, such a study would require significantly

[3] no sample is without biases, however the TOUGH sample attempts to eliminate a common bias in GRB host samples towards brighter host galaxies

more *HST* resources as it would need a full *HST* program, rather than a snapshot program as used to gather the data in this paper. We may have to wait for the completion of the first 30-40m class telescopes such as the *E-ELT*, as well as other major new observatories such as James Webb Space Telescope and *ALMA*, before we can fully probe these “missing” LGRB host galaxies.

3

Conclusions and future work

3.1 Conclusions

This thesis presents the first large sample of *HST* imaged LGRB host galaxies in the infra-red, with 40 imaged and 35 detected hosts, all with known redshifts $z < 3$. Furthermore, the location within the hosts of the LGRBs is known for 30 of these to within an *HST* pixel ($\sim 0.13''$), allowing these LGRBs to be analysed not just as a function of their hosts, but their locations within them.

Understanding the environments that give rise to LGRBs is crucial to understanding the LGRBs themselves, and this sample allows a look at not just the host galaxies that give rise to LGRBs but also the areas within the host galaxies that LGRBs come from. This thesis shows that LGRBs are much more likely to occur in the brightest regions of their hosts in the infra-red, similar to the result found by Fruchter et al. (2006) in the optical.

The morphology of the hosts is also analysed, and shows tentative evidence that in the infra-red LGRB host galaxies may appear more regular than in the optical. This is perhaps a sign that the typical LGRB host galaxy may be less irregular than previously thought, but that areas of high star-formation, brighter in the optical than the IR, may be causing the galaxy to appear to be more irregular than its underly morphology.

3.1.1 Future work

There is much more that could be done with the data presented in this thesis. It would be useful to compare this sample against (or possibly combine it with) others in different wavelengths, or even to compare it against samples of non-GRB hosting galaxies. It would also be interesting to see how the morphology and other paramaters of LGRB hosting galaxies evolves with time.

A

Appendix

References for table 2.1:

(1) Kelson & Berger, 2005 (2) De Pasquale et al., 2006 (3) Watson et al., 2006 (4) Fynbo et al., 2009 (5) Hjorth et al., 2012 (6) Sollerman et al., 2007 (7) Soderberg et al., 2005 (8) Mirabal & Halpern, 2006 (9) Cenko et al., 2006 (10) Prochaska et al., 2006 (11) Mirabal et al., 2006 (12) Cucchiara et al., 2006 (13) Ofek et al., 2006 (14) Bloom et al., 2006a (15) Jakobsson et al., 2007c (16) Price et al., 2006 (17) Thoene et al., 2006b (18) Levan et al., 2007 (19) Jakobsson et al., 2006 (20) Thoene et al., 2006a (21) Fynbo et al., 2007 (22) Jaunsen et al., 2007 (23) Jakobsson et al., 2007a (24) Perley et al., 2009 (25) Prochaska et al., 2007b (26) Cenko et al., 2007 (27) Prochaska et al., 2007a (28) Stern et al., 2007 (29) Ledoux et al., 2007 (30) Jakobsson et al., 2007b (31) Cucchiara et al., 2007 (32) Wiersema et al., 2008 (33) de Ugarte Postigo et al., 2008 (34) Cucchiara & Fox, 2008 (35) Jakobsson et al., 2008a (36) Fynbo et al., 2008a (37) Jakobsson et al., 2008c (38) Fynbo et al., 2008c (39) Perley et al., 2008 (40) Jakobsson et al., 2008b (41) Fynbo et al., 2008b (42) Vreeswijk et al., 2008 (43) Berger et al., 2008 (44) Cucchiara et al., 2008 (45) D'Elia et al., 2011 (46) Berger & Rauch, 2008 (47) Chornock et al., 2009a (48) Chornock et al., 2009b (49) Wiersema et al., 2009a (50)

Cenko et al., 2009 (51) Vergani et al., 2011 (52) Thoene et al., 2009 (53) Cucchiara et al., 2009 (54) Wiersema et al., 2009b.

References

Abraham R. G. et al., 1996, MNRAS, 279, L47

Basa S. et al., 2012, A&A, 542, A103

Belczynski K. et al., 2006, ApJ, 648, 1110

Berger E., 2009, ApJ, 690, 231

Berger E. et al., 2008, GRB Coordinates Network, 8335, 1

Berger E. et al., 2005a, GRB Coordinates Network, 3753, 1

Berger E. et al., 2005b, Nature, 438, 988

Berger E., & Rauch M., 2008, GRB Coordinates Network, 8542, 1

Bershady M. A. et al., 2000, AJ, 119, 2645

Bertin E., & Arnouts S., 1996, A&AS, 117, 393

Blaes O. et al., 1989, ApJ, 343, 839

Bloom J. S. et al., 2006a, GRB Coordinates Network, 5217, 1

Bloom J. S. et al., 2005, GRB Coordinates Network, 3758, 1

Bloom J. S. et al., 2009, ApJ, 691, 723

Bloom J. S. et al., 2006b, ApJ, 638, 354

Bloom J. S. et al., 1999, MNRAS, 305, 763

Boella G. et al., 1997, A&AS, 122, 327

Bouwens R. J. et al., 2011, Nature, 469, 504

Castro-Tirado A. J. et al., 2008, Nature, 455, 506

Cenko S. B. et al., 2006, GRB Coordinates Network, 4592, 1

Cenko S. B. et al., 2007, GRB Coordinates Network, 6888, 1

Cenko S. B. et al., 2012, ApJ, 753, 77

Cenko S. B. et al., 2009, GRB Coordinates Network, 9518, 1

Chornock R. et al., 2010, ArXiv e-prints

Chornock R. et al., 2009a, GRB Coordinates Network, 9151, 1

Chornock R. et al., 2009b, GRB Coordinates Network, 9243, 1

Christensen L. et al., 2004, A&A, 425, 913

Cline T. L. et al., 1980, ApJL, 237, L1

Cobb B. E., & Bailyn C. D., 2008, ApJ, 677, 1157

Cole S. et al., 2001, MNRAS, 326, 255

Conselice C. J., 2003, ApJS, 147, 1

Conselice C. J. et al., 2000, ApJ, 529, 886

Conselice C. J. et al., 2005, ApJ, 633, 29

Costa E. et al., 1997, Nature, 387, 783

Cucchiara A. et al., 2009, GRB Coordinates Network, 10202, 1

Cucchiara A., & Fox D. B., 2008, GRB Coordinates Network, 7654, 1

Cucchiara A. et al., 2007, GRB Coordinates Network, 7124, 1

Cucchiara A. et al., 2008, GRB Coordinates Network, 8346, 1

Cucchiara A. et al., 2011, ApJ, 736, 7

Cucchiara A. et al., 2006, GRB Coordinates Network, 5052, 1

De Pasquale M. et al., 2006, MNRAS, 365, 1031

de Ugarte Postigo A. et al., 2008, GRB Coordinates Network, 7650, 1

D'Elia V. et al., 2011, MNRAS, 418, 680

Ellis R. S. et al., 2013, ApJL, 763, L7

Evans P. A. et al., 2009, MNRAS, 397, 1177

Fishman G. J., 1999, A&AS, 138, 395

Fong W. et al., 2010, ApJ, 708, 9

Fruchter A. S. et al., 2006, Nature, 441, 463

Fruchter A. S. et al., 2000, ApJ, 545, 664

Fryer C. L. et al., 1999, ApJ, 526, 152

Fynbo J. et al., 2008a, GRB Coordinates Network, 7797, 1

Fynbo J. P. U. et al., 2009, ApJS, 185, 526

Fynbo J. P. U. et al., 2008b, GRB Coordinates Network, 8254, 1

Fynbo J. P. U. et al., 2008c, GRB Coordinates Network, 7949, 1

Fynbo J. P. U. et al., 2008d, ApJ, 683, 321

Fynbo J. P. U. et al., 2007, GRB Coordinates Network, 6759, 1

Gehrels N. et al., 2004, ApJ, 611, 1005

Gehrels N. et al., 2005, Nature, 437, 851

Gou L. J. et al., 2004, ApJ, 604, 508

Haensel P. et al., 1991, ApJ, 375, 209

Hjorth J., & Bloom J. S., 2012, The Gamma-Ray Burst - Supernova Connection, pp. 169–190

Hjorth J. et al., 2012, ApJ, 756, 187

Hopkins A. M., & Beacom J. F., 2006, ApJ, 651, 142

Jakobsson P. et al., 2007a, GRB Coordinates Network, 6398, 1

Jakobsson P. et al., 2008a, GRB Coordinates Network, 7757, 1

Jakobsson P. et al., 2006, GRB Coordinates Network, 5716, 1

Jakobsson P. et al., 2007b, GRB Coordinates Network, 7076, 1

Jakobsson P. et al., 2007c, GRB Coordinates Network, 6997, 1

Jakobsson P. et al., 2008b, GRB Coordinates Network, 8062, 1

Jakobsson P. et al., 2008c, GRB Coordinates Network, 7832, 1

Jarosik N. et al., 2011, ApJS, 192, 14

Jaunsen A. O. et al., 2007, GRB Coordinates Network, 6216, 1

Kaviraj S. et al., 2013, MNRAS, 429, L40

Kelly P. L. et al., 2008, ApJ, 687, 1201

Kelson D., & Berger E., 2005, GRB Coordinates Network, 3101, 1

Klebesadel R. W. et al., 1973, ApJL, 182, L85

Kouveliotou C. et al., 1993, ApJL, 413, L101

Le Floc'h E. et al., 2003, A&A, 400, 499

Ledoux C. et al., 2007, GRB Coordinates Network, 7023, 1

Levan A. J. et al., 2007, MNRAS, 378, 1439

Levesque E. M. et al., 2010, AJ, 140, 1557

Lu L. et al., 1996, ApJS, 107, 475

MacFadyen A. I., & Woosley S. E., 1999, ApJ, 524, 262

Madau P. et al., 1998, ApJ, 498, 106

Mazets E. P. et al., 1979, Nature, 282, 587

Mazzali P. A. et al., 2003, ApJL, 599, L95

Meegan C. A. et al., 1992, Nature, 355, 143

Meszaros P., 2001, Science, 291, 79

Meszaros P., & Rees M. J., 1993, ApJ, 405, 278

Metzger M. R. et al., 1997, Nature, 387, 878

Mirabal N., & Halpern J. P., 2006, GRB Coordinates Network, 4591, 1

Mirabal N. et al., 2006, ApJ, 643, L99

Narayan R. et al., 1992, ApJL, 395, L83

Ofek E. O. et al., 2006, GRB Coordinates Network, 5123, 1

Oke J. B., & Gunn J. E., 1983, ApJ, 266, 713

Paczynski B., 1986, ApJL, 308, L43

Paczynski B., 1991, AcA, 41, 257

Perley D. A. et al., 2009, AJ, 138, 1690

Perley D. A. et al., 2008, GRB Coordinates Network, 7962, 1

Price P. A. et al., 2006, GRB Coordinates Network, 5275, 1

Prochaska J. X. et al., 2006, GRB Coordinates Network, 4593, 1

Prochaska J. X. et al., 2007a, GRB Coordinates Network, 6890, 1

Prochaska J. X. et al., 2007b, GRB Coordinates Network, 6864, 1

Rees M. J., & Meszaros P., 1992, MNRAS, 258, 41P

Sahu K. C. et al., 1997, Nature, 387, 476

Salvaterra R. et al., 2009, Nature, 461, 1258

Savaglio S. et al., 2009, ApJ, 691, 182

Savaglio S. et al., 2005, ApJ, 635, 260

Schlafly E. F., & Finkbeiner D. P., 2011, ApJ, 737, 103

Smail I. et al., 2011, MNRAS, 414, L95

Soderberg A. M. et al., 2005, GRB Coordinates Network, 4186, 1

Sollerman J. et al., 2007, A&A, 466, 839

Stanek K. Z. et al., 2006, ACTAA, 56, 333

Stern D. et al., 2007, GRB Coordinates Network, 6928, 1

Stringer M. et al., 2011, MNRAS, 414, 1927

Svensson K. M. et al., 2010, MNRAS, 405, 57

Tanvir N. R. et al., 2009, Nature, 461, 1254

Tanvir N. R. et al., 2012, ApJ, 754, 46

Thoene C. C. et al., 2009, GRB Coordinates Network, 8889, 1

Thoene C. C. et al., 2006a, GRB Coordinates Network, 5812, 1

Thoene C. C. et al., 2006b, GRB Coordinates Network, 5373, 1

Tody D., 1993, in ASP Conf. Ser. 52: Astronomical Data Analysis Software and Systems II, Hanisch R. J., Brissenden R. J. V., Barnes J., eds., pp. 173+

Tremaine S., & Zytkow A. N., 1986, ApJ, 301, 155

Trenti M. et al., 2012, ApJL, 749, L38

Usov V. V., 1992, Nature, 357, 472

van Paradijs J. et al., 1997, Nature, 386, 686

Vergani S. D. et al., 2011, A&A, 535, A127

Vreeswijk P. et al., 2008, GRB Coordinates Network, 8301, 1

Watson D. et al., 2006, ApJ, 652, 1011

Wiersema K. et al., 2009a, GRB Coordinates Network, 9250, 1

Wiersema K. et al., 2008, GRB Coordinates Network, 7517, 1

Wiersema K. et al., 2009b, GRB Coordinates Network, 10263, 1

Wolf C., & Podsiadlowski P., 2007, MNRAS, 375, 1049

Woosley S. E., 1993a, ApJ, 405, 273

Woosley S. E., 1993b, ApJ, 405, 273

Woosley S. E., 1996, in American Institute of Physics Conference Series, Vol. 384, American Institute of Physics Conference Series, Kouveliotou C., Briggs M. F., Fishman G. J., eds., pp. 709–718

Woosley S. E., & Bloom J. S., 2006, ARA&A, 44, 507

Xu D. et al., 2013, ApJ, 776, 98